Neurogenesis Leads Early Development in Zebrafish

Zhengduo Wang[1], Li Tian[2] and Bo Li[1, *]
1. The Institute for Advanced Studies, Wuhan University, Wuhan 430072, P. R. China.
2. Department of Physics, Wenzhou University, Wenzhou 325000, P. R. China.
* Corresponding author. Email: libo@whu.edu.cn

Abstract: Vertebrate early neurogenesis is a highly conserved process fundamental to brain function and the emergence of intelligence. However, the cellular dynamics bridging gastrulation and organogenesis remain elusive due to observational challenges. We developed a live-cell imaging platform for transgenic zebrafish that provides, for the first time, a continuous reconstruction of early neurogenesis across subcellular to organismal scales. Our analysis reveals that neurogenesis is a precisely orchestrated process. Neuronal cell bodies initially coalesce into discrete, linearly arranged clusters extending from the brain along the spinal cord. From these hubs, axons radiate outward to innervate the central nervous system and peripheral tissues, including the yolk sac surface. A primary pioneer neuron projects from the brain, coursing ventrally in parallel to the body axis. Secondary neurons then interconnect, forming a pervasive network that is subsequently refined through selective axonal apoptosis. The emergence of frequent Ca^{2+} flashes only after structural maturation indicates that functionality is contingent upon an established scaffold. We also observe concurrent material transport and a slow, directional flow of Ca^{2+} along axons, suggesting complementary signaling modalities. Furthermore, neurogenesis exhibits precise spatiotemporal coupling with histogenesis, particularly with the developing lateral line and vasculature. Our work, with refined spatial and time resolution, defines the kinetic pathway of early neurogenesis and underscores the critical interplay of subsystems in embryogenesis, offering fundamental insights for neural health and bio-inspired intelligence.

The establishment of the nervous system, or neurogenesis, provides the structural foundation for brain function and organismal behavior [1-3]. Investigating this process *in vivo* is therefore of profound importance for understanding the brain and intelligence, thereby informing the design of artificial systems [4]. As a critical initiator and organizer of embryonic development, neurogenesis is also intricately coordinated with the organogenesis and histogenesis [5] of other tissues, knowledge of which offers a valuable interventional window for regenerative medicine [6]. However, the biological events occurring between germ layer formation and organogenesis—the primary period for neurogenesis—remain poorly defined, largely due to a lack of dynamic recording at fine temporal resolution. This absence of direct experimental observation bridging cellular and organismal scales currently impedes a comprehensive understanding of neurogenesis and its interplay with other developmental processes.

To elucidate the dynamics of neurogenesis, we employed long-term *in vivo* imaging to document early development in transgenic zebrafish from the zygote stage (**Figure 1a**). Transgenic lines were engineered to fluorescently label neural cells, Ca^{2+} activity, lateral line cells, vascular endothelium, slow muscle, and cardiomyocytes [7-12], enabling simultaneous visualization of neural architecture, brain function, and other tissues/organs (**Figures 1b, S1**). Zygotes were embedded in a hydrated agarose gel matrix under controlled conditions, supporting proper development to the juvenile stage. The experimental platform is schematically outlined in **Extended Data Figure 1**. The entire neurogenesis and organogenesis processes in 3D were recorded via spinning-disk and two-photon confocal microscopy (**Figure S2, Supplementary Movie 1**). With temporal resolution from 0.5 second to 72 hours and spatial coverage from subcellular to whole-organism scales, we systematically reconstructed neurogenesis with unprecedented detail and defined its relationship with organogenesis and histogenesis (**Figure 1c**). Embryos at various hours post-fertilization (hpf) were subjected to transcriptomic analysis to correlate in vivo observations with global gene expression patterns (**Figure S3**).

By targeting the developmental period that the neural system is established, which is also the period between germ layer formation and organogenesis, we identified key neurogenesis events and their functions. The initial neural structure comprises two neuronal somata clusters in the brain (**Figure 1d, e, Extended Data Figure 2a, Supplementary Movie 2**). Axons project from these clusters, forming nascent networks in the brain, yolk sac, and spinal cord (**Figure 1f, g, Extended Data Figure 2b, Supplementary Movie 3**). Subsequently, additional clusters emerge caudally, representing spinal cord precursors (**Figure 1e**). A major ventral neuron (MVN) extends from the brain, coursing parallel to the dorsal spinal cord to innervate somatic regions (**Figure 1h, i, Extended Data Figure 2c, Supplementary Movie 4**). This MVN exhibits spatial co-localization with the lateral line, underscoring neural system role in motor function establishment **(Figure 2a-e, Extended Data Figure 3a**). Notably, blood circulation initiates only after this neural scaffold forms, highlighting neurogenesis primacy in early development (**Figure 2f-h, Extended Data Figures 4, Supplementary Movie 5**). Hierarchical network assembly, guided by growth cones, dominates neurogenesis (**Figure 3, Extended Data Figure 7, Supplementary Movies 6, 7**). Subsequent structural optimization occurs through selective neuronal apoptosis (**Figure 4a-h, Extended Data Figure 8a-c, Supplementary Movie 8**). Finally, network maturation enables functionality, evidenced by delayed onset of Ca^{2+} transients (**Figure 4i-k, Supplementary Movie 9**) and slow-scale material transport (**Figure 4l-r, Extended Data Figure 8d, e, Supplementary Movie 10**). Our findings are schematically summarized in **Extended Data Figure 9**.

Initial stage of neurogenesis exhibits highly organized features.

Neural system development is spatiotemporally segregated into brain and spinal cord regions. To establish a unified timeline, we define t = 0 as the fertilization time point, maintained consistently throughout this study. Neural development initiates first in the brain region. By twelve hours post-fertilization, several neuronal somata coalesce, constituting the first organized structure of the nervous system (**Figure 1d, Extended Data Figure 2a, Supplementary Movie 2**). Two cell clusters emerge at the anteriormost aspect of the embryo, positioned bilaterally in the brain. The position of the cell clusters corresponds to the transient area between the midbrain and hindbrain, but is distal to the forebrain in the adult fish. The fluorescence intensity of these clusters increases dramatically around 20 hours (**Figure 1e**), indicating a rapid expansion in neuronal number.

Axons subsequently extend from these clustered somata, forming an interconnected network that encompasses both the brain and yolk sac regions (**Figure 1f, Extended Data Figure 2b, Supplementary Movie 3**). Notably, the yolk sac constitutes an integral component of this early neurogenesis. Rather than developing independently, extending axons first elaborate within the brain before projecting to colonize the yolk sac surface, ultimately forming a continuous network (**Figure 1f, Extended Data Figure 2b, Supplementary Movie 3**). Growth cones maintain a consistent extension rate of 0.9 μm/min throughout this process (**Figure 1g**). The transgenic zebrafish line utilizes the elavl3 promoter to drive EGFP expression. As elavl3 is a specific pan-neuronal marker, the observed signals unequivocally identify neural structures, excluding non-neural tissues such as epithelium. This confirms the yolk sac is actively innervated by brain-derived axons during neurogenesis.

Spinal cord neurogenesis initiates nearly concurrently with brain development. Shortly after the initial neuronal clusters form in the brain, additional clusters emerge along the embryonic axis, establishing the foundational framework for the spinal cord neural system (**Figure 1f, Extended Data Figure 2b**). Positioned dorsally, these structures are designated dorsal cell body clusters (DCBCs). Rather than appearing gradually in an anterior-posterior sequence, DCBCs exhibit a synchronous emergence at t = 20 hours (**Figure 1e, Extended Data Figure 2b, Supplementary Movie 3**), indicating coordinated development that precludes sequential anterior-to-posterior signaling. Subsequently, a singular growth cone projects ventrally from the brain cluster, extending caudally in a directed manner (**Figure 1h, Extended Data Figure 2c, Supplementary Movie 4**). This pioneering growth cone maintains approximately constant velocity (**Figure 1i**), establishing the major ventral neuron (MVN) that runs parallel to the dorsal DCBCs. This signaling for the process is thus along the anterior-to-posterior axis. Finally, branching axons interconnect DCBCs and the MVN, exhibiting precise spatial correspondence with somite boundaries. The signaling now converts into dorsal-to-ventral axis. These observations establish DCBCs and the MVN as the structural framework for spinal cord neural architecture, upon which subsequent axonal networks are elaborated.

Transcriptomic analysis corroborates the in vivo observations (**Figure 1j-m**). Biological process enrichment underscores early synaptic signaling (**Figure 1j**), while cellular component analysis reveals emphasis on foundational neural structures and GABAergic receptor complexes (**Figure 1k**). Molecular function enrichment highlights key activities including serine/threonine

phosphatase, ion channel, and transporter functions (**Figure 1l**). Pathway analysis further confirms the prominence of initial synaptic transmission processes (**Figure 1m**). Collectively, these KEGG enrichment results demonstrate that by 12 hpf, zebrafish embryonic neural development is at the foundational stage of functional activation, characterized by established molecular catalysis, substance transport, and nascent synapse formation.

Interplay between neurogenesis with histogenesis, and organogenesis.

Neurogenesis proceeds in concert with histogenesis, the process of cellular differentiation into tissues. To delineate their relationship, we simultaneously visualized biomarkers for neurogenesis and stem cell differentiation via immunostaining for Sox2 (stemness) and elavl3 (neurogenesis) in embryos at various post-fertilization timepoints. As early as 3 hours post-fertilization, Sox2 is strongly expressed at the animal pole (**Fig. 2a - 3 hours**). The neural marker signal emerges approximately 16 hours later, initially coexisting with the stem cell marker. Subsequently, elavl3 and Sox2 signals exhibit complex spatiotemporal coupling in their distribution (**Fig. 2a**).

Immunostaining at 48 hpf reveals that elevated Sox2 expression exhibits strong spatial co-localization with the MVN (**Fig. 2b**), which further overlaps with the lateral line (cldnb) (**Extended Data Figure 3a**). A longitudinal domain of high Sox2 expression aligns precisely with the MVN tract. Multiple spherical Sox2+ cell clusters are interconnected by this Sox2+ domain, corresponding to the MVN and lateral line (**Fig. 2b**). These discrete Sox2+ clusters localize to the brain, yolk sac periphery, and spinal cord regions (**Fig. 2c**). The co-localization of Sox2, MVN, and lateral line persists from 48 to 72 hpf (**Extended Data Figure 3b, c**), demonstrating sustained synergy between neurogenesis and stem cell differentiation.

Sox2, a key developmental regulator, is established to coordinate stemness maintenance [13] and cell cluster formation [14]. Our observations unequivocally demonstrate spatially organized interplay between Sox2 and neural system development. Notably, at t = 3 hours, when Sox2 expression initiates, neural cells remain undifferentiated. As Sox2 marks both embryonic stem cells and neural progenitor cells, this occurrence sequence implies histogenesis could offer regulatory signaling for early neurogenesis (**Fig. 2a**). Paradoxically, the organized $Sox2^{+}$ domain and clusters only emerge at t = 48 hours after MVN and spinal cord structures mature (**Fig. 2c, Extended Data Figures 3b, c**), suggesting neurogenesis subsequently directs histogenesis. Weighted gene co-expression network analysis identifies genes involved in both processes (**Fig. 2d**). Their temporal expression patterns validate our *in vivo* observations—genes predominantly responsible for stem cell differentiation precede those primarily governing neuronal growth (**Fig. 2e**).

Anatomically, the MVN co-localizes with the lateral line, indicating that neurogenesis directs the establishment of mechanosensory capability (**Extended Data Figure 3a**). The Sox2+ bulges exhibit complete overlap with the lateral line cell clusters responsible for force sensing [15]. Our *in vivo* observations thus provide direct evidence that Sox2 mediates lateral line development, corroborating earlier reports [16, 17]. In contrast, actin expression demonstrates markedly weaker spatial correlation with elavl3 (neuronal), Sox2 (stemness), or cldnb (lateral line) markers (**Extended Data Figure 3d**). As a cytoskeletal protein typically expressed in terminally

differentiated cells like epithelium [18], the ectopic actin expression pattern suggests it is regulated by Sox2 rather than serving as a driver—a conclusion supported by molecular evidence [19].

Subsequently, blood circulation is established throughout the embryo. The developing vasculature revolves around cardiac function, forming a network that intimately intertwines with neural architecture (**Fig. 2f**). Both live imaging and growth factor expression confirm neural system development precedes vasculogenesis (**Fig. 2f, g**). The circulatory system ultimately organizes into three distinct circuits within the brain, yolk sac, and spinal cord regions (**Fig. 2h, Extended Data Figure 4, Supplementary Video 5**). Notably, we observe highly directional blood cell flow across the yolk sac surface (**Fig. 2h, Extended Data Figure 4, Supplementary Video 5**). These findings support a model wherein the yolk sac contributes to early development not merely through nutrient provision, but by facilitating organized mass transport via nascent vascular networks. Pharmaceutical inhibition with LY294002, a classical angiogenesis inhibitor [20], simultaneously disrupts both neural and vascular development (**Extended Data Figure 5**), confirming these systems share crucial signaling pathways [21].

To delineate the sequence of neurogenesis and organogenesis, we fixed transgenic zebrafish embryos at distinct developmental stages. These lines feature fluorescent labeling of marker genes for vascular endothelium (**Figure S1a**), neurons (**Figure S1b**), lateral line (**Figure S1c**), cardiomyocytes (**Figure S1d**), skeletal muscle (**Figure S1e**), and Ca^{2+} activity (**Figure S1f**), where fluorescence onset marks the initiation of each process. Simultaneous phase-contrast imaging captured other organ formation. Sequential analysis verifies that neural system development, coupled with histogenesis (including Sox2 expression, lateral line formation, actin patterning, and muscle differentiation) (**Figs. 2a, b, Extended Data Figs. 3, 6a**), initiates approximately 4 hours prior to angiogenesis and organogenesis (**Figure 2f, Extended Data Figure 6b-d**), and 30 hours before detectable neural activity (**Figure 4i-p**). As a pervasive network, the early neuronal architecture provides positional guidance for organ placement and vascular patterning, substantiating neurogenesis as the pioneering event in embryonic development.

Network establishment dominates neural development.

Neurogenesis is governed by the establishment and maturation of axonal networks extending from neuronal somata clusters. In both brain and spinal cord regions, select growth cones exhibit directed migration. These pioneer growth cones establish major axons that form the primary neural framework (**Figures 3a, 3l, Extended Data Figure 7, Supplementary Movies 6, 7**). Secondary axons subsequently branch from these primary pathways, elaborating the network complexity (**Figures 3a, 3l, Extended Data Figure 7, Supplementary Movies 6, 7**). In the brain, major axons project from initial clusters to other brain regions or the yolk sac (**Figure 3a, Extended Data 7a, Supplementary Movie 6**), whereas spinal cord axons extend along the dorsal-to-ventral axis (**Figure 3l, Extended Data 7b, Supplementary Movie 7**).

To correlate growth cone dynamics with network topology, we implemented Strahler number analysis [22] for brain and yolk sac axons. Higher Strahler values indicate greater axonal convergence (major pathways), while lower values represent terminal branches. The evolving probability distribution of Strahler values quantitatively captures network maturation (**Fig. 3b**). Anatomically, higher-order axons exhibit larger diameters (**Fig. 3c**), consistent with observations

in the brain of drosophila melanogaster [23]. Structurally, major axons maintain smaller angular deviations from growth cone trajectories than branching axons (**Fig. 3d**), reflecting functional specialization. Intermediate Strahler values, namely rank 2 and 3, display bimodal angular distributions (**Fig. 3e**), suggesting their transitional role in network connectivity. Dynamically, growth cones exhibit directed migration rather than stochastic exploration (**Fig. 3f**), resulting in highly aligned major axon orientation. Concurrently, growth cone velocity decays significantly over time (**Fig. 3g**), consistent with chemotactic mechanisms dependent on chemical gradients. Neural network establishment coincides with node number saturation and negligible growth cone speeds (**Fig. 3g**).

Transcriptomic profiles corroborate these *in vivo* observations. By 24 hpf, neural development transitioned from foundational patterning to specialized maturation, with synchronized enhancement of neuronal identity and synaptic function. Biological process and pathway analyses highlighted neuronal differentiation in both peripheral and central nervous systems, alongside strengthened synaptic signaling (**Figs. 3h, 3i**). At 48 hpf, development advanced to a stage of structural refinement and functional maturation, characterized by precise axonal morphogenesis and synaptic transmission. Consistent with this, Gene ontology and pathway enrichment revealed significant upregulation of axon development and guidance processes (**Figs. 3j, 3k**).

The kinetic pathway of network establishment in the spinal cord closely mirrors that of the brain. In concert with the caudal extension of the major ventral axon, multiple growth cones emerge from dorsal cell clusters, exhibiting dorsal-to-ventral trajectories (**Fig. 3l, Extended Data 7b, Supplementary Movie 7**). Secondary axons with more stochastic orientations subsequently elaborate the network (**Fig. 3m-o**). Notably, as the MVN elongates, other major axons reorient from strict dorsal-to-ventral alignment to trajectories parallel with the MVN (**Fig. 3p**). This reorientation suggests these axons establish connectivity with the MVN and are guided by its extension - a kinetic pathway absent in the brain-yolk sac system due to the lack of an analogous migratory traction force or signaling source.

Structural pruning by apoptosis precedes neural function.

During the late stages of network establishment, both *in vivo* observation and transcriptomic analysis indicate the frequent occurrence of apoptosis in specific neurons within the brain and yolk sac. During neuronal apoptosis, intense Ca^{2+} transients propagate throughout the entire axon (**Fig. 4a, Extended Data Figure 8a-c, Supplementary Movie 8-left**). The frequency of apoptosis initially increases, peaking at 36 hours post-fertilization (**Fig. 4b**). This peak coincides with the period of network structural consolidation, implying a role for apoptosis in network optimization. Transcriptomic data reveal concurrent upregulation of genes related to cell death, neurogenesis, and Ca^{2+} signaling, although no gene across all three categories is annotated in current database (**Fig. 4c**). Ca^{2+} signaling has previously been implicated in apoptosis in cell lines [24, 25]. Our observation not only confirms this phenomenon *in vivo*, but also elucidate its potential biological function to be pruning the axonal network. Biological process and pathway enrichment confirm the neural system is undergoing structural refinement and functional adaptation, with enhancements in axonal morphology and synaptic precision (**Fig. 4d, e**). We therefore hypothesize that apoptosis refines the network by eliminating suboptimal connections, thereby maximizing information transfer efficiency.

To test this, we analyzed the characteristics of apoptosing neurons. Pruned neurons consistently exhibit two features: a higher Strahler order and a significant deviation in their orientation from the original growth cone trajectory (**Fig. 4f, g**). Following network completion, apoptosis persists at a lower frequency (**Figure 4h, Supplementary Movie 8-right**). However, neurons eliminated at this stage are markedly more mature. As exemplified in **Fig. 4h**, the Ca^{2+} transient can propagate across the entire yolk sac via a single, intricately branched neuron. The loss of such mature neurons induces more extensive structural compromise and carries a higher metabolic cost, which partly explains the observed reduction in apoptosis rate after network finalization.

Beginning at 36 hours post-fertilization, Ca^{2+} transients initiate within neuronal somata (**Fig. 4i, Supplementary Movie 9**), with their frequency increasing over time (**Fig. 4j**). As Ca^{2+} is a key mediator of neural signaling and a hallmark of neuronal activity [26], its emergence only after network structural maturity supports the principle that function is contingent upon established architecture. Notably, these Ca^{2+} transients occur not only in the brain but also across the yolk sac surface, which is now populated with neuronal cell bodies (**Fig. 4k**). Given the absence of elavl3 signal in the yolk sac at 20 hpf (**Fig. 1d**), these neurons cannot be yolk sac-native. Since axons previously projected from brain clusters to innervate the yolk sac (**Fig. 1f**), we thus posit a testable hypothesis that these somata result from neuronal migration from the brain.

Besides somatic Ca^{2+} transients, we observe mass transport along axons. Particulate structures, slightly larger than axonal diameters, move bidirectionally within axonal tracts (**Fig. 4l, Extended Data Figure 8d, e, Supplementary Movie 10**) at velocities orders of magnitude slower than electrical signals [27] or calcium sparks [28], identifying a novel transport phenomenon. Its occurrence in both elavl3:EGFP and elavl3:GCaMP6f lines at similar speeds (**Fig. 4m**) suggests these moving entities are highly localized Ca^{2+} waves. The number of transported particles increases dramatically (**Fig. 4n**), mirroring the rise in Ca^{2+} transient frequency . The direction of transportation is not random: anisotropic in the brain (**Fig. 4p**) and predominantly dorsoventral in the spinal cord (**Fig. 4o**). This implies that chemotactic gradients guide not only growth cones [29] but also material transport. By 72 hpf, the neural system reaches a state of functional maturation and homeostasis, with fully developed structure and activity (**Fig. 4q, r**).

Summary and Discussion

In this work, we have elucidated zebrafish neurogenesis through a comprehensive *in vivo* imaging approach. Multi-channel imaging across temporal and spatial scales reveals the leading role of neurogenesis in early development, occurring concomitantly with histogenesis yet preceding organogenesis (**Extended Data Figure 9**). This distinctly orchestrated process unfolds through four sequential stages: somata clustering, network establishment, apoptosis-mediated optimization, and functional maturation. We have identified stereotypical phenomena during each stage, revealing potential early targets for brain health maintenance and Alzheimer's disease intervention [30].

The neural system strategies revealed here provide fundamental insights into the developmental origins of intelligence and offer practical guidance for artificial intelligence design. Essentially, we can construct artificial systems using living organisms as blueprints. The observed pattern—

where axons extend after somata form base-station-like clusters—ensures optimal mapping between neural architecture and body plan. The timing of apoptosis-mediated optimization is particularly noteworthy: its peak immediately follows network establishment, when neuronal arbors remain relatively simple, minimizing structural and metabolic costs. While persisting at lower levels later, this strategic pruning demonstrates sophisticated system-level intelligence in balancing information efficiency against energy expenditure. The delayed initiation of organ function after neural network establishment effectively prevents developmental dysfunction—a principle directly applicable to brain-inspired computing systems [31].

These findings raise critical questions for future investigation. First, the signaling pathways underlying the observed phenomena require molecular dissection at finer temporal resolution. Second, the material basis and functional significance of the slow transport phenomena demand clarification. Third, how network refinement and aging influence behaviors like swimming [32] merits exploration, particularly regarding neural-organ coordination. Finally, developing additional transgenic lines targeting early developmental regulators like Sox2 will further illuminate the coupling between stem cell differentiation and neurogenesis.

Methods.

Construction and maintenance of transgenetic zebrafish lines. Zebrafish strains (elavl3:GCaMP6f) and (elavl3:YFP) were acquired from the China Zebrafish Resource Center (http://www.zfish.cn/), whereas the (elavl3:EGFP) and (fli-1:mCherry) strains were purchased from Nanjing Ezerinka Biotechnology Co., Ltd. (http://www.ezerinka.com/). The hybrid lines (elavl3:GCaMP6f; elavl3:YFP) and (elavl3:EGFP; fli-1:mCherry) were generated in-house through crossbreeding and selective rearing. All zebrafish were maintained in a recirculating aquaculture system procured from Nanjing Ezerinka Biotechnology Co., Ltd.

The system temperature was set to 28 °C, with continuous operation of UV sterilization and oxygen supply. A 5% sea salt solution and 5% sodium bicarbonate solution were used to regulate conductivity and ion balance, maintaining system conductivity between 500–800 μS/cm and pH between 7.0–8.0. Ambient temperature was controlled at 28 °C using air conditioning, and a 12 h light/12 h dark photoperiod was applied [33]. Approximately one-third of the system water was replaced daily to keep total ammonia nitrogen below 0.02 mg/L.

To facilitate subsequent spawning, male and female zebrafish were housed separately. Males were distinguished by their slender body shape, flat abdomen, and lemon-yellow coloration, whereas females exhibited a fuller body, rounded abdomen, and silvery-gray pigmentation, allowing reliable visual sex identification. Adult zebrafish were fed live Artemia nauplii daily. The hatching procedure was as follows: 5 g of Artemia cysts and 5 g of sea salt were added to 1 L of pure water. The mixture was aerated under illumination for 24 h, after which aeration was stopped to allow eggshells to separate. The hatched nauplii settled at the bottom and were collected for feeding. Fish were fed 1-2 times per day, with the amount adjusted to ensure consumption within 15-20 minutes.

Sample preparation for in vivo zebrafish imaging. On the day before imaging, female and male zebrafish of different transgenic strains were placed in spawning tanks separated by a divider. The tanks were filled with a 1:1 mixture of fresh water and system water, covered, and maintained overnight. On the following morning, after the onset of illumination, the divider was removed to allow direct interaction between males and females. Males began nudging the abdominal region of the females, which subsequently initiated spawning. Approximately 30 minutes later, both females and males were returned to the main rearing system. The fertilized eggs were collected from the spawning tanks into 10 cm Petri dishes and maintained in specialized zebrafish embryo medium at 28 °C [33].

Embryo imaging typically commenced around 24 hours post-fertilization (hpf). Prior to imaging, embryos were screened using a spinning disk confocal microscope, and only those exhibiting clear fluorescence signals were selected for further processing. The chorion was then removed from each embryo to improve imaging quality. Although the chorion serves as a protective barrier during early development, it limits imaging depth and introduces motion artifacts as embryos become more active inside the membrane. For dechorionation, 24-hpf embryos were transferred to a Petri dish with a small amount of water and placed under a stereomicroscope. A small incision was made in the chorion using a corneal scissors, and the embryo was gently extruded with fine forceps.

The dechorionated embryos were then transferred to a confocal imaging dish. Low-melting-point agarose (0.12 g) was dissolved in 10 mL of ddH_2O by microwave heating to prepare a 1.2% solution [34]. After cooling to approximately 35 °C, the agarose solution was dispensed over the embryos. The position and orientation of each embryo were adjusted with forceps before the agarose solidified. For imaging at earlier developmental stages, such as 12 hours post-fertilization (hpf), the chorion was not removed due to the structural fragility of the embryos at this period, as mechanical manipulation could readily cause damage. Instead, the embryos within their intact chorions were directly embedded in low-melting-point agarose for immobilization during imaging.

Live cell imaging. Live imaging of zebrafish embryos was performed using a Spin SR10 spinning disk confocal microscope (Evident Olympus) equipped with an Oko-lab incubation chamber (H301-MINI). The system maintained a constant temperature of 28 °C throughout the experiments. Embryos were mounted in confocal dishes (Nest, 801001) and imaged with typical laser intensity set at 20% and exposure time at 200 ms. For fluorescence excitation, the 488 nm laser line was used to visualize pan-neuronal labels in the transgenic lines (elavl3:EGFP and elavl3:GCaMP6f), while the 514 nm laser was employed for imaging the (elavl3:YFP) line.

To enhance experimental throughput, approximately 20 embryos were placed in each confocal dish. The microscope's positional memory function was utilized to record individual embryo locations, enabling simultaneous time-lapse acquisition from multiple specimens. All embryos were imaged using axial Z-stack acquisition mode with the following parameters. Z-stack imaging was performed with a 60x oil objective at 100 μm Z-range and 2-3 μm step size, a 30x oil objective at

150 μm Z-range and 2-3 μm step size, and a 10x objective at 400 μm Z-range and 10 μm step size, respectively. Time-series imaging was performed at 20-minute intervals over a total duration of 48 hours, generating continuous 3D volumetric data throughout the recording period [35-37].

Immunostaining Experiments. Zebrafish embryos at various developmental stages were collected after spawning and fixed with 4% paraformaldehyde (PFA; Pumeike, PMK0240) at room temperature for 2 hours. The chorions of the embryos were then carefully removed under a stereomicroscope. After repeated washing with PBS, the samples were permeabilized with 0.1% Triton X-100 (Solarbio, T8200-500ml) for 30 minutes at room temperature. Subsequently, blocking was performed using 3% bovine serum albumin (BSA; Pumeike, PMK0181-250g) containing 0.1% Triton X-100 for 2 hours at room temperature.

The embryos were incubated overnight at 4 °C in the dark with a SOX2 primary antibody (abcam, ab97959) diluted 1:500 in 3% BSA to label pluripotent stem cells and neural stem cells at early developmental stages [38]. The following day, the antibody solution was removed, and the samples were washed three times with PBS (10 minutes per wash). Thereafter, the samples were incubated overnight at 4 °C in the dark with a mixture of Goat Anti-Rabbit IgG H&L (Alexa Fluor® 594; abcam, ab150080) [39] and Hoechst 33258 [40], both diluted 1:1000 in PBS. Finally, the samples were washed three times with PBS (10 minutes each), followed by two additional PBS washes, and then mounted on confocal dishes for imaging.

Pharmaceutical Interference. The PI3K inhibitor LY294002 [41, 42] (MedChemExpress, HY-10108; supplied as a 10 mM solution in DMSO) was employed to investigate the PI3K/Akt signaling pathway. This pathway is a critical downstream component of both VEGF-driven angiogenesis, which promotes endothelial cell survival, proliferation, and migration, and neurotrophin signaling (e.g., NGF and BDNF), which is essential for neuronal survival and axonal growth. Accordingly, LY294002 disrupts these processes by inhibiting PI3K. For the experiments, a 1 mM stock solution was prepared by diluting the compound in DMSO. This stock was further diluted in zebrafish embryo medium to obtain working concentrations of 10, 50, and 100 μM. Zebrafish embryos were exposed to these solutions, and their neuronal and vascular development was assessed after 24 hours of treatment.

Data reconstruction and 3D visualization. Whole-embryo imaging of the zebrafish neural network was performed using an Evident FVMPE-RS multiphoton laser scanning microscope. At 24 hours post-fertilization, zebrafish embryos (elavl3:EGFP) were dechorionated under a stereomicroscope and embedded in 1.2% low-melting-point agarose mounted at the bottom of a confocal dish, using either live or 4% PFA-fixed specimens. Image acquisition was carried out with a 25x water-immersion objective and a dedicated two-photon lens. Tiling was employed to cover the entire embryonic neural network, with Z-stacks acquired at 10 μm intervals, spanning a total depth of approximately 600 μm. The resulting datasets were processed using Olympus imaging software for three-dimensional reconstruction. Alternatively, Z-stack images were

imported into Imaris (Oxford Instruments) for further 3D rendering and visualization.

Analysis of live cell imaging data. Time-lapse imaging data of zebrafish neural network development were analyzed using Fiji (ImageJ). Growth cone dynamics, including migration trajectories and velocity, were quantified with the Manual Tracking plugin [43]. The analysis workflow consisted of the following steps: Time-lapse image stacks were loaded into Fiji, and the Manual Tracking plugin was initialized with appropriate temporal intervals and spatial calibration based on the acquisition settings. Growth cones were manually selected and tracked across consecutive frames using the plugin's point-and-click interface. The plugin automatically recorded their positional coordinates over time and computed kinematic parameters such as displacement, velocity, and persistence. To assess structural organization within the developing network, angular relationships between neurites were also measured using Fiji's built-in angle measurement tool. Specific neurite segments and growth cone orientations were manually annotated, and their relative angles were calculated to evaluate network topology and directional guidance. All tracking and angular data were exported for further statistical analysis and graphical representation in GraphPad Prism.

Transcriptome sequencing and analysis. Zebrafish embryos at key developmental time points (12, 24, 36, 48, 60, and 72 hours post-fertilization) were collected and immediately preserved in TRIzol reagent. Total RNA was extracted following the manufacturer's protocol, and RNA integrity was verified prior to sequencing. All transcriptome sequencing services were provided by Shanghai Ji Kai Gene Technology Co., Ltd. The resulting gene expression matrices across time points were subjected to subsequent bioinformatic analysis. Time-series gene clustering was performed using the online platform bioinformatics.com.cn with the Mfuzz package, which identifies genes with similar expression dynamics throughout development. Clusters exhibiting neural-related expression patterns were selected for further functional annotation.

Gene set enrichment analysis was carried out using R software (v4.2.1) with the clusterProfiler package. Neural-associated highly expressed genes from distinct developmental windows were analyzed for KEGG [44] pathway enrichment. Significantly enriched terms were identified across multiple functional categories, including Biological Process (BP), Molecular Function (MF), and Cellular Component (CC), with a focus on pathways related to neural development, synaptic transmission, and axon guidance. Visualization of temporal expression trends and functional enrichment results was conducted using ggplot2 [45] in R, enabling clear representation of dynamic transcriptome changes during embryonic neural development.

References:

1. Götz, M. & Huttner, W. B. The cell biology of neurogenesis. *Nat Rev Mol Cell Biol* **6**, 777-788 (2005). https://doi.org/10.1038/nrm1739
2. Turrigiano, G. G. & Nelson, S. B. Homeostatic plasticity in the developing nervous system. *Nat Rev Neurosci* **5**, 97-107 (2004). https://doi.org/10.1038/nrn1327

3. Roth, G. & Dicke, U. Evolution of the brain and intelligence. *Trends Cogn Sci* **9**, 250-257 (2005). https://doi.org/10.1016/j.tics.2005.03.005
4. McCulloch, W. S. & Pitts, W. A logical calculus of the ideas immanent in nervous activity. 1943. *Bull Math Biol* **52**, 99-115; discussion 173-197 (1990).
5. 5 Campos-Ortega, J. A. & Hartenstein, V. in *The Embryonic Development of Drosophila melanogaster* 85-164 (Springer Berlin Heidelberg, 1985).
6. Burns, T. C. & Quinones-Hinojosa, A. Regenerative medicine for neurological diseases-will regenerative neurosurgery deliver? *Bmj* **373**, n955 (2021). https://doi.org/10.1136/bmj.n955
7. Park, H. C. *et al.* Analysis of upstream elements in the HuC promoter leads to the establishment of transgenic zebrafish with fluorescent neurons. *Dev Biol* **227**, 279-293 (2000). https://doi.org/10.1006/dbio.2000.9898
8. Dunn, T. W. *et al.* Brain-wide mapping of neural activity controlling zebrafish exploratory locomotion. *Elife* **5**, e12741 (2016). https://doi.org/10.7554/eLife.12741
9. Aman, A. & Piotrowski, T. Wnt/beta-catenin and Fgf signaling control collective cell migration by restricting chemokine receptor expression. *Dev Cell* **15**, 749-761 (2008). https://doi.org/10.1016/j.devcel.2008.10.002
10. Lawson, N. D. & Weinstein, B. M. In vivo imaging of embryonic vascular development using transgenic zebrafish. *Dev Biol* **248**, 307-318 (2002). https://doi.org/10.1006/dbio.2002.0711
11. Elworthy, S., Hargrave, M., Knight, R., Mebus, K. & Ingham, P. W. Expression of multiple slow myosin heavy chain genes reveals a diversity of zebrafish slow twitch muscle fibres with differing requirements for Hedgehog and Prdm1 activity. *Development* **135**, 2115-2126 (2008). https://doi.org/10.1242/dev.015719
12. Peng, X. Y. *et al.* [Construction and assessment of heart-specific green fluorescence zebrafish line]. *Yi Chuan* **35**, 511-518 (2013). https://doi.org/10.3724/sp.j.1005.2013.00511
13. Pevny, L. H. & Nicolis, S. K. Sox2 roles in neural stem cells. *Int J Biochem Cell Biol* **42**, 421-424 (2010). https://doi.org/10.1016/j.biocel.2009.08.018
14. Liu, Z. *et al.* 3D imaging of Sox2 enhancer clusters in embryonic stem cells. *Elife* **3**, e04236 (2014). https://doi.org/10.7554/eLife.04236
15. Faucherre, A., Pujol-Martí, J., Kawakami, K. & López-Schier, H. Afferent neurons of the zebrafish lateral line are strict selectors of hair-cell orientation. *PLoS One* **4**, e4477 (2009). https://doi.org/10.1371/journal.pone.0004477
16. Germanà, A. *et al.* Sox-2 in taste bud and lateral line system of zebrafish during development. *Neurosci Lett* **467**, 36-39 (2009). https://doi.org/10.1016/j.neulet.2009.09.056
17. Undurraga, C. A. *et al.* Sox2 and Sox3 are essential for development and regeneration of the zebrafish lateral line. *bioRxiv*, 856088 (2019).
18. Jodoin, J. N. *et al.* Stable Force Balance between Epithelial Cells Arises from F-Actin Turnover. *Dev Cell* **35**, 685-697 (2015). https://doi.org/10.1016/j.devcel.2015.11.018

19. Feng, R. & Wen, J. Overview of the roles of Sox2 in stem cell and development. *Biol Chem* **396**, 883-891 (2015). https://doi.org/10.1515/hsz-2014-0317
20. Secchiero, P. *et al.* TRAIL promotes the survival and proliferation of primary human vascular endothelial cells by activating the Akt and ERK pathways. *Circulation* **107**, 2250-2256 (2003). https://doi.org/10.1161/01.Cir.0000062702.60708.C4
21. Elorza Ridaura, I., Sorrentino, S. & Moroni, L. Parallels between the Developing Vascular and Neural Systems: Signaling Pathways and Future Perspectives for Regenerative Medicine. *Adv Sci (Weinh)* **8**, e2101837 (2021). https://doi.org/10.1002/advs.202101837
22. Zhao, A. *et al.* Eye structure shapes neuron function in Drosophila motion vision. *Nature* **646**, 135-142 (2025). https://doi.org/10.1038/s41586-025-09276-5
23. Liao, M., Liang, X. & Howard, J. The narrowing of dendrite branches across nodes follows a well-defined scaling law. *Proc Natl Acad Sci U S A* **118** (2021). https://doi.org/10.1073/pnas.2022395118
24. Rintoul, G. L., Raymond, L. A. & Baimbridge, K. G. Calcium buffering and protection from excitotoxic cell death by exogenous calbindin-D28k in HEK 293 cells. *Cell Calcium* **29**, 277-287 (2001). https://doi.org/10.1054/ceca.2000.0190
25. Wang, S. H., Shih, Y. L., Ko, W. C., Wei, Y. H. & Shih, C. M. Cadmium-induced autophagy and apoptosis are mediated by a calcium signaling pathway. *Cell Mol Life Sci* **65**, 3640-3652 (2008). https://doi.org/10.1007/s00018-008-8383-9
26. Zong, W. *et al.* Fast high-resolution miniature two-photon microscopy for brain imaging in freely behaving mice. *Nat Methods* **14**, 713-719 (2017). https://doi.org/10.1038/nmeth.4305
27. Rama, S., Zbili, M. & Debanne, D. Signal propagation along the axon. *Curr Opin Neurobiol* **51**, 37-44 (2018). https://doi.org/10.1016/j.conb.2018.02.017
28. Cheng, H. & Lederer, W. J. Calcium sparks. *Physiol Rev* **88**, 1491-1545 (2008). https://doi.org/10.1152/physrev.00030.2007
29. Mortimer, D., Fothergill, T., Pujic, Z., Richards, L. J. & Goodhill, G. J. Growth cone chemotaxis. *Trends Neurosci* **31**, 90-98 (2008). https://doi.org/10.1016/j.tins.2007.11.008
30. Jiang, Q. *et al.* Antiageing strategy for neurodegenerative diseases: from mechanisms to clinical advances. *Signal Transduct Target Ther* **10**, 76 (2025). https://doi.org/10.1038/s41392-025-02145-7
31. Kagan, B. J. *et al.* In vitro neurons learn and exhibit sentience when embodied in a simulated game-world. *Neuron* **110**, 3952-3969.e3958 (2022). https://doi.org/10.1016/j.neuron.2022.09.001
32. Burke, S. N. & Barnes, C. A. Neural plasticity in the ageing brain. *Nat Rev Neurosci* **7**, 30-40 (2006). https://doi.org/10.1038/nrn1809
33. Nasiadka, A. & Clark, M. D. Zebrafish breeding in the laboratory environment. *ILAR journal* **53**, 161-168 (2012).
34. Geng, Y. & Peterson, R. T. Rapid mounting of zebrafish larvae for brain imaging.

Zebrafish **18**, 376-379 (2021).
35. Ewald, A. J., Werb, Z. & Egeblad, M. Dynamic, long-term in vivo imaging of tumor-stroma interactions in mouse models of breast cancer using spinning-disk confocal microscopy. *Cold Spring Harb Protoc* **2011**, pdb.top97 (2011). https://doi.org/10.1101/pdb.top97
36. Gintoli, M. *et al.* Spinning disk-remote focusing microscopy. *Biomed Opt Express* **11**, 2874-2888 (2020). https://doi.org/10.1364/boe.389904
37. Hayashi, S. & Okada, Y. Ultrafast superresolution fluorescence imaging with spinning disk confocal microscope optics. *Mol Biol Cell* **26**, 1743-1751 (2015). https://doi.org/10.1091/mbc.E14-08-1287
38. Xiao, Y. *et al.* Dopey2 and Pcdh7 orchestrate the development of embryonic neural stem cells/ progenitors in zebrafish. *iScience* **26**, 106273 (2023). https://doi.org/10.1016/j.isci.2023.106273
39. Perez, Y. *et al.* Mutations in the microtubule-associated protein MAP11 (C7orf43) cause microcephaly in humans and zebrafish. *Brain* **142**, 574-585 (2019). https://doi.org/10.1093/brain/awz004
40. Bazhulina, N. P. *et al.* Binding of Hoechst 33258 and its derivatives to DNA. *J Biomol Struct Dyn* **26**, 701-718 (2009). https://doi.org/10.1080/07391102.2009.10507283
41. Gharbi, S. I. *et al.* Exploring the specificity of the PI3K family inhibitor LY294002. *Biochem J* **404**, 15-21 (2007). https://doi.org/10.1042/bj20061489
42. Jiang, H., Fan, D., Zhou, G., Li, X. & Deng, H. Phosphatidylinositol 3-kinase inhibitor(LY294002) induces apoptosis of human nasopharyngeal carcinoma in vitro and in vivo. *J Exp Clin Cancer Res* **29**, 34 (2010). https://doi.org/10.1186/1756-9966-29-34
43. Fabrice CordeliÔøΩres, I. C., Orsay. *Manual Tracking*, <https://imagej.net/ij/plugins/track/track.html> (2005).
44. Kanehisa, M., Furumichi, M., Sato, Y., Kawashima, M. & Ishiguro-Watanabe, M. KEGG for taxonomy-based analysis of pathways and genomes. *Nucleic Acids Res* **51**, D587-d592 (2023). https://doi.org/10.1093/nar/gkac963
45. Wickham, H. ggplot2. *Wiley interdisciplinary reviews: computational statistics* **3**, 180-185 (2011).

Acknowledgments: We thank Tao Tan for helpful discussions; Peishi Wang and Mingyang Chen for helping maintain the transgenetic zebrafish lines; Runjie Yu and Siyi Zhang from Oujiang Laboratory for assistance in spinning disk confocal and two photon microscopy imaging, respectively; and Deepseek for text polishing. This study was supported by taxpayers of China through National Natural Science Foundation of China (distinguished young scholars funding, overseas) and Wuhan University (talents startup funding).

Author contributions. B.L. conceptualized the project, B.L. Z.D.W. designed the research, Z.D.W, L.T. and B.L. performed experiments, Z.D.W. analyzed the data. All authors discussed the results and wrote the paper.

Competing interests. The authors declare no competing interests.

Additional information

Extended data is available for this paper after the main text.

Supplementary information is available for this paper at a separate file.

Reprints and permissions information are available at

Correspondence and requests for materials should be addressed to B.L. (libo@whu.edu.cn)

Data availability The data and analysis code that support the findings of this study are available upon reasonable request to B.L..

Figure Captions.

Figure 1. Initial stages of zebrafish neurogenesis. a, Summary of zebrafish embryonic developmental timeline and associated events in this study. The abbreviations for various events are as follows: Cluster: The developmental stage at which neuronal somata begin to aggregate, forming the initial basal structure during early neural development in zebrafish embryos; Network: The developmental stage when the neural network begins to form in zebrafish embryos; Optimization: The developmental stage during neural network formation in zebrafish embryos, characterized by the apoptosis of certain network structures to refine and optimize the overall neural circuitry; Ca^{2+} Flashing and Transport: The developmental stage in zebrafish embryos when the neural network is initially established, marked by prominent Ca^{2+} transients in brain neurons and active material transport within the neural network; Muscle: The developmental stage at which distinct skeletal slow muscles become observable in zebrafish embryos; Heart: The developmental stage when cardiac muscle becomes detectable in zebrafish embryos; Vascular: The developmental stage at which blood circulation is observed in zebrafish embryos; Lateral line: The developmental stage when the lateral line neuromasts become visible during zebrafish embryonic development. **b,** Vectors used for generating transgenic zebrafish lines. All zebrafish employed in this study were generated; using the Tol2 transposon system. **c,** Schematic diagram of early neural development in zebrafish embryos. The left panel shows the lateral view, and the right panel shows the dorsal view. Neuronal somata are depicted in purple, and red arrows indicate the direction of neural network growth. **d,** Representative confocal image of early neural development in a zebrafish embryo (elavl3:EGFP), with the inset showing a magnified view of clustered neuronal cell bodies. scale bar=200μm. **e,** The number of clusters (red dashed line) and the optical signal intensity of the predominant brain cluster (black solid line) as a function of time during the initiation of neural development in zebrafish embryos. **f,** Representative confocal micrographs of early neural network formation in zebrafish (elavl3: EGFP) embryos at 24 hours post-fertilization. Green fluorescence indicates pan-neuronal labeling. The image was acquired using a 30x objective, scale bar=50μm.

g, Growth cone velocity as a function of time during neural network development in zebrafish embryos. **h,** Representative confocal image illustrating neurite outgrowth from the brain toward the spinal cord during neural development in a zebrafish embryo (elavl3:EGFP). scale bar=100μm. **i,** The growth rate of the primary ventral nerve from the brain to the spinal cord over time during neural development in zebrafish embryos. **j-m,** KEGG enrichment analysis of neural-related transcriptome data from zebrafish embryos at 12 hpf. **j,** Biological process terms: 1-10 correspond to chemical synaptic transmission, anterograde trans-synaptic signaling, trans-synaptic signaling, synaptic signaling, regulation of membrane potential, circadian rhythm, regulation of circadian rhythm, glycogen metabolic process, glucan metabolic process, and cellular glucan metabolic process. **k,** Cellular component terms: 1-10 correspond to postsynapse, postsynaptic membrane, chloride channel complex, synaptic membrane, SMN-Sm protein complex, Cajal body, GABA-A receptor complex, GABA receptor complex, somatodendritic compartment, and spliceosomal complex. **l,** Molecular function terms: 1-10 correspond to protein threonine phosphatase activity, protein serine phosphatase activity, protein serine/threonine phosphatase activity, phosphoprotein phosphatase activity, phosphoric ester hydrolase activity, phosphatase activity, extracellular ligand-gated ion channel activity, amino acid: sodium symporter activity, amino acid: cation symporter activity, and transmitter-gated ion channel activity. **m,** Pathway analysis terms: 1-10 correspond to mRNA surveillance pathway, neuroactive ligand-receptor interaction, oocyte meiosis, regulation of actin cytoskeleton, other glycan degradation, adrenergic signaling in cardiomyocytes, vascular smooth muscle contraction, insulin signaling pathway, cellular senescence, and herpes simplex virus 1 infection. For all statistical plots, unpaired Student's t-test ($n > 3$ experiments, data are mean $\pm$ SD) was conducted for all data. The error bars are the standard error of the mean of the data.

Figure 2. Coupling between neurogenesis with histogenesis and organogenesis. a, Representative immunofluorescence images of the nervous system and Sox2 in zebrafish embryos (elavl3:EGFP) at 3, 12, 24, and 36 hours of development. Sox2 is labeled in red, nuclei are counterstained with Hoechst (blue), and pan-neuronal labeling is shown by EGFP signal (green) in the transgenic line. Scale bars =100 μm. **b,** Immunofluorescence analysis of the nervous system and Sox2 in zebrafish embryos (elavl3:EGFP) at 48 h. Overview image. Scale bar =100 μm. **c,** Higher-magnification views of the boxed regions in **b**. Scale bars =50 μm. The color scheme is identical to that in **a**. **d,** Venn diagrams showing the overlap between neuro-related genes and stem cell-related genes (top), as well as between neuro-related genes and vascular-related genes (bottom), based on transcriptomic data. **e,** Normalized expression of Sox2, Sox3, Sox1b, Ntn1a, and Ntn1b genes at different developmental time points of zebrafish embryos from transcriptome data. **f,** Representative confocal image of early neural and vascular development in a zebrafish embryo. Green fluorescence labels pan-neuronal structures; red fluorescence marks vascular endothelium. Green arrows indicate neuronal signals; red arrows indicate vascular signals, scale bar=100μm. **g,** Normalized expression of Vegfab and Vegfaa genes at different developmental time points of zebrafish embryos from transcriptome data. **h,** Representative confocal images showing nervous and vascular development in a zebrafish embryo at 30 h, obtained from a cross between

elavl3:EGFP and fli1a:mCherry transgenic lines. The right panels display bright-field, vascular (mCherry), and neuronal (EGFP) images of the brain, yolk sac, and spinal cord regions. The leftmost confocal image was acquired with a 10x objective lens. Scale bars =200 μm. The three sets of images on the right were obtained using a 30x objective lens. Scale bars =50 μm. For all statistical plots, unpaired Student's t-test (n > 3 experiments, data are mean ± SD) was conducted for all data. The error bars are the standard error of the mean of the data.

Figure 3. Network formation in the brain and spinal cord regions. a, Representative confocal micrographs of early neural network formation in zebrafish (elavl3: EGFP) embryos at 24 hours post-fertilization. Green fluorescence indicates pan-neuronal labeling. The image was acquired using a 60× objective, scale bar=20μm. **b,** Frequency distribution of different network hierarchy levels during neural circuit assembly in zebrafish embryos. An axon directly connected to a growth cone is defined as Level 1; Level 2 denotes axons formed by the convergence of two Level 1 axons; Level 3 arises from the merging of two Level 2 axons. When a higher-level and a lower-level axon converge, the resulting axon retains the level of the higher one. **c,** Quantification of axonal widths across different orders. The inset displays the brightness profiles of low- and high-order axons. **d,** Statistical analysis of the angle between the direction of movement of growth cones and axons of different hierarchical levels. **e,** Polar plot showing the probability distribution of the angles between growth cone and axon movement directions. **f,** Representative confocal image of a growing growth cone, scale bar=20μm. **g,** Temporal changes in growth cone migration speed (black line) and the number of neural network nodes (red line). **h, i,** Enrichment analysis of neural-related highly expressed genes in 24 h zebrafish embryos: **h,** Biological process terms: 1-10 correspond to peripheral nervous system neuron axonogenesis, chemical synaptic transmission, anterograde trans-synaptic signaling, trans-synaptic signaling, synaptic signaling, peripheral nervous system development, peripheral nervous system neuron development, peripheral nervous system neuron differentiation, spinal cord development, and central nervous system neuron differentiation, respectively. **i,** Signaling pathway terms: 1-10 represent mRNA surveillance pathway, autophagy-other, neuroactive ligand-receptor interaction, oocyte meiosis, tight junction, adrenergic signaling in cardiomyocytes, Notch signaling pathway, virion-Ebolavirus/Lyssavirus/Morbillivirus, TGF-beta signaling pathway, and glycosphingolipid biosynthesis-ganglio series. **j, k,** Enrichment analysis of neural-related highly expressed genes in 48 h zebrafish embryos: **j,** Biological process terms: 1-10 correspond to cell projection morphogenesis, cell part morphogenesis, neuron projection morphogenesis, plasma membrane bounded cell projection morphogenesis, axon development, axonogenesis, heterophilic cell-cell adhesion via plasma membrane cell adhesion molecules, cell morphogenesis involved in neuron differentiation, regulation of vascular endothelial growth factor receptor signaling pathway and vascular endothelial growth factor signaling pathway. **k,** Signaling pathway terms: 1-7 represent Neuroactive ligand signaling, Cell adhesion molecules, Virion-Lassa virus and SFTS virus, Notch signaling pathway, Virion-Ebolavirus, Lyssavirus and Morbillivirus, ErbB signaling pathway and Glycosphingolipid biosynthesis -ganglio series. **l,** Representative confocal micrograph showing the formation of early neural networks in the spinal cord region of a transgenic zebrafish embryo

(Tg(elavl3:EGFP)) at 24 hours post-fertilization (hpf). The green fluorescence indicates pan-neuronal labeling. The top image was acquired with a 30× objective. Scale bar = 50 μm. **m,** Hierarchy of network integration in the developing spinal cord. The plot shows the distribution of axon ranks, defined by their origin: Rank 1 (direct from growth cones), Rank 2 (from two Rank 1), and Rank 3 (from two Rank 2). Fusion events always preserve the higher rank. **n,** Angular relationship between growth cone and axon trajectories. The graph statistically compares the direction angles across different hierarchical axon ranks. **o,** Directional alignment probability. The polar plot illustrates the distribution of angles between the movement vectors of growth cones and axons. **p,** Statistical analysis of the angles between the network extending from neuronal somata adjacent to the spinal cord and the direction of growth cone movement at different time points during spinal neural network development. For all statistical plots, unpaired Student's t-test ($n > 3$ experiments, data are mean ± SD) was conducted for all data with **** $P < 0.0001$, *** $P < 0.001$, ** $P < 0.1$, * $P < 0.5$, ns $P > 0.5$. The error bars are the standard error of the mean of the data.

Figure 4. Apoptosis assisted network optimization and brain function after network maturation. a, Representative confocal images showing the refinement of a subset of axonal networks via apoptosis during neural circuit formation in zebrafish (elavl3: GCaMP6f) embryos. White arrows indicate pruned axons. Scale bar = 50μm. **b,** Quantification of apoptosis events at different developmental time points in zebrafish embryos. **c,** Venn diagram showing the overlap among highly expressed neuro-related, calcium-related, and cell death-related genes from transcriptome data analysis of zebrafish embryos. **d, e,** Enrichment analysis of highly expressed death-related genes in 60 hpf zebrafish embryos. **d,** Biological process terms:1-10 correspond to positive regulation of apoptotic process, positive regulation of programmed cell death, positive regulation of cell death, regulation of apoptotic process, regulation of programmed cell death, regulation of cell death, apoptotic signaling pathway, extrinsic apoptotic signaling pathway,MyD88-dependent toll-like receptor signaling pathway, and extrinsic apoptotic signaling pathway via death domain receptors. **e,** Signaling pathway terms:1-10 represent Herpes simplex virus 1 infection, apoptosis, cytokine–cytokine receptor interaction, autophagy–animal, necroptosis,p53signaling pathway, Salmonella infection, cytoskeleton in muscle cells, virion – Ebolavirus/Lyssavirus/Morbillivirus, and MAPK signaling pathway. **f,** Statistical analysis of the angles between apoptotic versus non-apoptotic neurons and the axonal network in the zebrafish neural network. **g,** Probability of neuronal apoptosis events involving neurons of hierarchy level >2 in the developing zebrafish embryonic neural network. **h,** Representative confocal image (right) and corresponding structural diagram (left) of large-scale neural network apoptosis in a relatively mature zebrafish embryonic neural network. Red and green dashed circles indicate locations of the highest hierarchy axons; purple lines denote higher-level axonal projections. **i,** Representative confocal images showing calcium transients in a zebrafish (elavl3:GCaMP6f) embryo at 24 hpf (left) and 60 hpf (right), the right panel shows magnified views. Line chart showing the dynamics of cerebral neuronal calcium signals in zebrafish embryos at 24 and 60 hpf. Scale bar = 50μm. **j,** Statistical analysis of calcium flash frequency at different developmental stages of zebrafish embryos. **k,** Representative confocal image showing calcium transients observed on the yolk sac

surface of a zebrafish embryo (elavl3:GCaMP6f) at 60 hpf. Scale bar=50μm. **l,** Representative confocal images showing putative material transport within the axonal network of zebrafish (elavl3: GCaMP6f) embryos at approximately 48 hpf. Arrows indicate observed transported cargo. The inset shows the locations of transported cargo within the same axonal network at different time points. The position of the cargo is indicated by the grayscale value. **m,** Quantification of cargo transport velocity within the axonal network of zebrafish embryos (elavl3: GCaMP6f; elavl3: EGFP). The black dashed line denotes the average velocity of growth cone migration, and the red dashed line represents the average signal conduction velocity in myelinated axons. **n,** Quantification of cargo transport duration per unit time observed in the neural network at different time points during zebrafish embryonic development. **o,** Bar graph showing the probability of observed cargo transport directions within the neural network, comparing dorsal-to-ventral transport against all other directions. **p,** Polar histogram of cargo transport direction probabilities. **q, r,** Enrichment analysis of neural-related highly expressed genes in 60 hpf zebrafish embryos. **q,** Biological process terms: 1-10 correspond to chemical synaptic transmission, anterograde trans-synaptic signaling, trans-synaptic signaling, synaptic signaling, regulation of membrane potential, cholinergic synaptic transmission, positive regulation of developmental process, chloride transmembrane transport, chloride transport, and positive regulation of cell differentiation. **r,** Signaling pathway terms: e1-e6 represent Neuroactive ligand-receptor interaction, Cell adhesion molecules, Glycosphingolipid biosynthesis – ganglio series, Oocyte meiosis, Autophagy-other, and VEGF signaling pathway. For all statistical plots, unpaired Student's t-test ($n > 3$ experiments, data are mean ± SD) was conducted for all data with **** $P < 0.0001$, *** $P < 0.001$, ** $P < 0.1$, * $P < 0.5$, ns $P > 0.5$. The error bars are the standard error of the mean of the data.

Extended Date Figure 1. Schematics of the experimental design. An integrated approach of live imaging and transcriptomics was employed. First, zebrafish embryos were prepared by dechorionation and mounting in agarose for stable long-term imaging under controlled environmental conditions. Following this, time-lapse image data were acquired and analyzed. Concurrently, transcriptome sequencing was performed on embryos collected at different developmental stages. Finally, the imaging dynamics and gene expression data were correlated to identify potential functional links.

Extended Data Figure 2. Raw images of initial stages at a finer time scale. a, Time-series confocal micrographs of a Tg(elavl3:EGFP) zebrafish embryo during the initial phase of neurogenesis, acquired at a high temporal resolution (20-minute intervals). EGFP signal (green) labels neurons. Scale bar= 200 μm. **b,** Time-lapse confocal imaging (20-minute intervals) of a Tg(elavl3:EGFP) embryo, showing the extension of neural networks from cerebral neuronal somata toward the brain, spinal cord, and yolk sac. EGFP signal (green) marks neurons. Scale bar=50 μm. **c,** Representative high-temporal-resolution confocal images (20-minute intervals) capturing the caudal growth of the primary ventral nerve toward the spinal cord in a Tg(elavl3:EGFP) embryo during neural development. Neurons are visualized by EGFP fluorescence (green). Scale bar= 100 μm.

Extended Data Figure 3. Interplay between neurogenesis and embryo differentiation. a, Confocal images of a 48 hpf Tg(cldnb:lynEGFP) embryo stained for Sox2. Red, Sox2; green, lynEGFP (lateral line nerves); blue, Hoechst (nuclei). The top panel (scale bar=200 μm) and higher-magnification views of the boxed region below (30x objective; scale bar=50 μm) are presented. **b,** Representative confocal micrographs of a 24 hpf Tg(elavl3:EGFP) zebrafish embryo immunolabeled for Sox2. Red, Sox2; green, EGFP (neurons); blue, Hoechst (nuclei). The leftmost image was acquired with a 10x objective (scale bar=100 μm); others with a 30x objective (scale bar= 50 μm). **c,** Immunolocalization of Sox2 in a 36 hpf Tg(elavl3:EGFP) embryo. Magenta, Sox2; green, EGFP (neurons); blue, Hoechst (nuclei). The leftmost panel (10x objective; scale bar=100 μm) and subsequent panels (30x objective; scale bar, 50 μm) are shown. **d,** Time course of actin distribution in Tg(elavl3:EGFP) embryos. Representative confocal micrographs at 3, 12, 24, and 48 hpf immunolabeled for actin. Red, actin; green, EGFP (neurons); blue, Hoechst (nuclei). For each time point, the left image is a 10x overview (scale bar=100 μm), and the right images are 30x magnifications .scale bar=50 μm.

Extended Data Figure 4. Coevolution of neural networks and blood vessels. Representative confocal images showing nervous and vascular development in a zebrafish embryo at 48h, obtained from a cross between elavl3:EGFP and fli-1:mCherry transgenic lines. The right panels display bright-field, vascular (mCherry), and neuronal (EGFP) images of the brain, yolk sac, and spinal cord regions. The leftmost confocal image was acquired with a 10x objective lens. Scale bars =200 μm. The three sets of images on the right were obtained using a 30x objective lens. Scale bars =50 μm.

Extended Data Figure 5. Pharmaceutical interference on network formation. a, Representative confocal images of zebrafish embryos following 24-hour treatment with LY294002 at concentrations of 10 μM, 50 μM, and 100 μM. The embryos are from a double transgenic Tg(elavl3:EGFP; fli-1:mCherry) line, with green fluorescence labeling neurons and red fluorescence labeling blood vessels. Scale bar = 100 μm.

Extended Data Figure 6. Relationship between neurogenesis and organogenesis. a, Representative confocal microscopy images of live zebrafish (smyhc1:EGFP) embryos. Skeletal muscle is labeled with green fluorescent protein (GFP). The white arrow indicates the time point and location of distinct skeletal muscle signals during embryonic development. Scale bar = 100 μm. **b,** Representative confocal microscopy images of live zebrafish (cmlc2:EGFP) embryos. Cardiac muscle is labeled with GFP. The white arrow indicates the time point and location of distinct cardiac muscle signals during embryonic development. Scale bar = 100 μm. **c,** Representative confocal microscopy images of live zebrafish (elavl3:EGFP) embryos. Pan-neuronal structures are labeled with GFP. The white arrow indicates the time point and location of distinct neuronal signals during embryonic development. Scale bar = 100 μm. **d,** Representative confocal microscopy images of live zebrafish (elavl3:EGFP; fli-1:mCherry) embryos. Pan-

neuronal structures are labeled with GFP, and vascular endothelium is labeled with mCherry. The white arrow indicates the time point and location of distinct vascular signals during embryonic development. Scale bar = 100 μm.

Extended Data Figure 7. Rew images of the network formation in both brain and spinal cord at a finer time scale. a, Representative confocal images showing the dynamic process of neural network formation on the zebrafish brain and yolk sac surface at higher temporal resolution. The time interval between the two images is 20 minutes. Scale bar = 20 μm. **b,** Representative confocal images illustrating the dynamic process of neural network formation in the zebrafish spinal cord at higher temporal resolution. The time interval between the two images is 20 minutes. Scale bar = 50 μm.

Extended Data Figure 8. More examples of apoptosis and brain functions. a-c, Representative time-series confocal images showing partial neural networks undergoing apoptosis during neural development in zebrafish. White arrows indicate neural networks undergoing apoptosis. Scale bars: 50 μm in **a** and **c**, 20 μm in **b**. **d, e,** Representative confocal images of cargo transport in the mature neural network of transgenic zebrafish embryos. Panels show the **d** elavl3:EGFP and **e** elavl3:GCaMP6f lines. For each, the left image provides a low-magnification overview. The scale bar is 50 μm, and the right image is a higher-magnification view of the boxed region, with transported cargo indicated by white arrows. The scale bar is 10 μm.

Extended Data Figure 9. Schematic summary of the findings. In this study, we pioneered the use of live 3D imaging to reconstruct the complete timeline of neural network development and organogenesis in zebrafish. We found that neural network initiation involves the appearance of base station-like clusters in the brain and spinal cord, from which networks extend to cover the brain, spinal cord, and yolk sac. This network is subsequently refined via an apoptosis-like pruning process. Once established, the network displays frequent somatic calcium transients and active material transport in neurons.

Supplementary Information for "Neurogenesis Leads Early Development in Zebrafish"

Zhengduo Wang[1], Li Tian[2] and Bo Li[1, *]
3. The Institute for Advanced Studies, Wuhan University, Wuhan 430072, P. R. China.
4. Department of Physics, Wenzhou University, Wenzhou 325000, P. R. China.
* Corresponding author. Email: libo@whu.edu.cn

This PDF file includes:

Supplementary text

Figure S1 to S3

Tables S1to S2

SI References

Legends for Movies S1 to S10

Caption for Figures S1 to S3

Other supplementary materials for this manuscript include the following:

Movies S1 to S10

I. Characterization of transgenetic zebrafish lines.

The zebrafish strains used in this study are summarized in **Table S1**. Transgenic zebrafish lines were genotyped by examining the expression pattern of fluorescent proteins. Specifically, embryos at 48 hours post-fertilization (hpf) were observed under a fluorescence microscope, and the correct integration of the transgene was verified based on the specific localization of the fluorescent signal. For the identification of different transgenic zebrafish lines, we assessed the fluorescence expression in corresponding 48-hour-old embryos under a confocal microscope (**Figure S1**), and assessed the key morphological features.

In the Tg(fli-1:mCherry) [1] line, the endothelial-specific promoter drives the expression of a red fluorescent protein, enabling visualization of the vascular system. As shown in Fig. S1a, distinct vascular-like structures were observed in the brain, heart, and spinal cord of zebrafish embryos. Blood cell flow within the vessels was also visible under bright-field microscopy, confirming correct labeling of this line. The Tg(elavl3:EGFP) [2] line utilizes a pan-neuronal-specific promoter fused with green fluorescent protein to visualize the nervous system. As demonstrated in Fig. S1b, strong EGFP expression was detected in the brain and spinal cord, with clearly visible neuronal somata and axonal networks, indicating proper labeling. In the Tg(cldnb:lynEGFP) [3] line, a lateral line system-specific promoter drives membrane-localized EGFP expression for visualization of the lateral line. Fig. S1c shows high EGFP signals in a rosette-like pattern at the lateral line positions along the spinal cord, confirming accurate labeling. The Tg(cmlc2:EGFP) [4] line expresses EGFP under a cardiomyocyte-specific promoter to visualize the heart. As observed in Fig. S1d, robust green fluorescence was present in the cardiac region, along with visible heartbeats, verifying correct labeling. In the Tg(smyhc1:EGFP) [5] line, a slow muscle-specific promoter drives EGFP expression for skeletal muscle visualization. Fig. S1e shows strong fluorescence in the spinal region with clearly defined muscle fibers, confirming proper labeling. The Tg(elavl3:GCaMP6f) [6] line uses a pan-neuronal promoter to express the calcium indicator GCaMP6f, enabling visualization of neural calcium dynamics. As shown in Fig. S1f, high fluorescence was observed in the brain and spinal cord, with discernible neuronal somata, axonal networks, and dynamic fluorescence fluctuations, indicating correct labeling.

Table S1. Zebrafish strains used in this study.

ID	Name	Description	Excitation wavelength [nm]
1	Tg(elavl3:EGFP)	Visualize the Nervous System	488
2	Tg(elavl3:GCaMP6f)	Visualize of Neural Calcium Ion Signals	488
3	Tg(fli-1:mCherry)	Visualize Blood Vessels	561

4	Tg(cldnb:lynEGFP)	Visualize Lateral Line Neuromast	488
5	Tg(smyhc1: EGFP)	Visualize Skeletal Muscle	488
6	Tg(cmlc2: EGFP)	Visualize Cardiac Muscle	488
7	Zebrafish(AB)	Wild-Type Zebrafish	N.A

II. Imaging reconstruction and data analysis.

The reconstruction of imaging stacks from confocal microscopy is conducted using Cell Sens Dimension Desktop 4.2.1 (https://lifescience.evidentscientific.com.cn/en/software/cellsens/). In the top planar view, the Maximum Intensity Projection (MIP) algorithm is adopted to overlay all images in the z-stack into a single image. In the side view, the Marching Cubes (Surface Reconstruction Algorithms) algorithm is used to yield the stereoscopic spheroids (**Fig. S3**). Compared with the range in the xy plane, the length scale in z is relatively small, making the analysis based on xy projection reasonably accurate.

III. Verification and analysis of transcriptomic data.

Zebrafish embryos were collected at 12, 24, 36, 48, 60, and 72 hours post-fertilization (hpf). Approximately ten embryos per time point were immediately placed in RNase-free tubes containing TRIzol reagent and subsequently sent to GeneChem (Shanghai, China) for RNA sequencing. The resulting transcriptomic data were analyzed in our laboratory.

The resulting gene expression matrices across time points were subjected to subsequent bioinformatic analysis (**Figure S3**). Time-series gene clustering was performed using the online platform bioinformatics.com.cn with the Mfuzz package, which identifies genes with similar expression dynamics throughout development. Clusters exhibiting neural-related expression patterns were selected for further functional annotation. Gene set enrichment analysis was carried out using R software (v4.2.1) with the cluster Profiler package. Neural-associated highly expressed genes from distinct developmental windows were analyzed for KEGG pathway enrichment. Significantly enriched terms were identified across multiple functional categories, including Biological Process (BP), Molecular Function (MF), and Cellular Component (CC), with a focus on pathways related to neural development, synaptic transmission, and axon guidance. Visualization of temporal expression trends and functional enrichment results was conducted using ggplot2 in R, enabling clear representation of dynamic transcriptome changes during embryonic neural development.

IV. Pharmaceutical interference experiment.

The chemical compounds, antibodies, and live-cell dyes employed are listed in **Table 2**. LY294002

is a broad-spectrum PI3K inhibitor targeting PI3Kα, PI3Kδ, and PI3Kβ with IC_{50} values of 0.5, 0.57, and 0.97 μM, respectively [7-9]. It also inhibits casein kinase 2 (CK2) and acts as a competitive DNA-PK inhibitor, binding reversibly to its kinase domain with an IC_{50} of 1.4 μM [7]. As an apoptosis inducer [10], LY294002 impairs neural [11] and vascular development primarily through suppression of the PI3K/Akt signaling pathway. In neural development, it attenuates the anti-apoptotic activity of Akt, leading to increased neuronal cell death, particularly among embryonic neural precursors [11]. Furthermore, it disrupts neuronal migration [12] and differentiation [13], resulting in mislocalization and altered cell fate specification, which ultimately compromises neural circuit assembly. Axonal outgrowth and synaptogenesis are also suppressed due to impaired cytoskeletal reorganization and growth cone dynamics [14, 15]. In vascular development, LY294002 inhibits [16] by blocking VEGF-induced Akt activation, thereby reducing angiogenic output [17]. It also interferes with EC migration [17] and vascular branching [18] by dampening chemotactic responses and motility, and undermines vessel stability by reducing pericyte coverage, leading to fragile and dysfunctional vasculature. Consistent with these mechanisms, our experimental data show that treatment of zebrafish embryos with 100 μM LY294002 for 24 hours significantly elevated embryonic lethality and delayed both neural and vascular development.

Table S2. Reagents used in this work.

ID	Name	Manufacturer	Catalog Number
1	LY294002	MCE	HY-10108
2	SiR-actin Kit	Cytoskeleton	CY-SC001
3	Hoechst 33258	Pumei Biological	PMK0965
4	Anti-SOX2	Abcam	ab97959
5	IgG H&L (Alexa Fluor® 594)	Abcam	ab150080

SI References

1. Lawson, N. D. & Weinstein, B. M. In vivo imaging of embryonic vascular development using transgenic zebrafish. *Dev Biol* **248**, 307-318 (2002). https://doi.org/10.1006/dbio.2002.0711
2. Park, H. C. *et al.* Analysis of upstream elements in the HuC promoter leads to the establishment of transgenic zebrafish with fluorescent neurons. *Dev Biol* **227**, 279-293 (2000). https://doi.org/10.1006/dbio.2000.9898
3. Aman, A. & Piotrowski, T. Wnt/beta-catenin and Fgf signaling control collective cell migration by restricting chemokine receptor expression. *Dev Cell* **15**, 749-761 (2008). https://doi.org/10.1016/j.devcel.2008.10.002
4. Peng, X. Y. *et al.* [Construction and assessment of heart-specific green fluorescence zebrafish line]. *Yi Chuan* **35**, 511-518 (2013). https://doi.org/10.3724/sp.j.1005.2013.00511

5. Elworthy, S., Hargrave, M., Knight, R., Mebus, K. & Ingham, P. W. Expression of multiple slow myosin heavy chain genes reveals a diversity of zebrafish slow twitch muscle fibres with differing requirements for Hedgehog and Prdm1 activity. *Development* **135**, 2115-2126 (2008). https://doi.org/10.1242/dev.015719
6. Dunn, T. W. *et al.* Brain-wide mapping of neural activity controlling zebrafish exploratory locomotion. *Elife* **5**, e12741 (2016). https://doi.org/10.7554/eLife.12741
7. Chaussade, C. *et al.* Evidence for functional redundancy of class IA PI3K isoforms in insulin signalling. *Biochem J* **404**, 449-458 (2007). https://doi.org/10.1042/bj20070003
8. Davidson, D., Amrein, L., Panasci, L. & Aloyz, R. Small Molecules, Inhibitors of DNA-PK, Targeting DNA Repair, and Beyond. *Front Pharmacol* **4**, 5 (2013). https://doi.org/10.3389/fphar.2013.00005
9. Gharbi, S. I. *et al.* Exploring the specificity of the PI3K family inhibitor LY294002. *Biochem J* **404**, 15-21 (2007). https://doi.org/10.1042/bj20061489
10. Jiang, H., Fan, D., Zhou, G., Li, X. & Deng, H. Phosphatidylinositol 3-kinase inhibitor(LY294002) induces apoptosis of human nasopharyngeal carcinoma in vitro and in vivo. *J Exp Clin Cancer Res* **29**, 34 (2010). https://doi.org/10.1186/1756-9966-29-34
11. Crowder, R. J. & Freeman, R. S. Phosphatidylinositol 3-kinase and Akt protein kinase are necessary and sufficient for the survival of nerve growth factor-dependent sympathetic neurons. *J Neurosci* **18**, 2933-2943 (1998). https://doi.org/10.1523/jneurosci.18-08-02933.1998
12. Zhang, Q. *et al.* BDNF promotes EGF-induced proliferation and migration of human fetal neural stem/progenitor cells via the PI3K/Akt pathway. *Molecules* **16**, 10146-10156 (2011). https://doi.org/10.3390/molecules161210146
13. Lee, J. E., Lim, M. S., Park, J. H., Park, C. H. & Koh, H. C. S6K Promotes Dopaminergic Neuronal Differentiation Through PI3K/Akt/mTOR-Dependent Signaling Pathways in Human Neural Stem Cells. Mol Neurobiol 53, 3771-3782 (2016). https://doi.org/10.1007/s12035-015-9325-9
14. Qian, Y. et al. Maslinic acid promotes synaptogenesis and axon growth via Akt/GSK-3β activation in cerebral ischemia model. Eur J Pharmacol 764, 298-305 (2015). https://doi.org/10.1016/j.ejphar.2015.07.028
15. Read, D. E. & Gorman, A. M. Involvement of Akt in neurite outgrowth. Cell Mol Life Sci 66, 2975-2984 (2009). https://doi.org/10.1007/s00018-009-0057-8
16. Secchiero, P. et al. TRAIL promotes the survival and proliferation of primary human vascular endothelial cells by activating the Akt and ERK pathways. Circulation 107, 2250-2256 (2003). https://doi.org/10.1161/01.Cir.0000062702.60708.C4
17. Maekawa, H. et al. Ephrin-B2 induces migration of endothelial cells through the phosphatidylinositol-3 kinase pathway and promotes angiogenesis in adult vasculature. Arterioscler Thromb Vasc Biol 23, 2008-2014 (2003). https://doi.org/10.1161/01.Atv.0000096655.56262.56
18. Qi, J. H. et al. Phosphoinositide 3 kinase is critical for survival, mitogenesis and migration but not for differentiation of endothelial cells. Angiogenesis 3, 371-380 (1999).

https://doi.org/10.1023/a:1026565908445

Legends for Supplementary Movies

Movie S1. Two-photon imaging and 3D reconstruction of the nervous system in a zebrafish (elavl3:EGFP) embryo. A 30 hpf zebrafish embryo was immobilized in low-melting-point agarose and imaged with a two-photon microscope (FVMPE-RS) equipped with a 25x water-immersion objective. Z-stacks were acquired with a 5 μm step size.

Movie S2. Wide-field time-lapse confocal imaging of initial neural development in a zebrafish (elavl3:EGFP) embryo. Images were captured using a 30x silicon oil-immersion objective with tiling. Pan-neuronal structures are labeled with EGFP (excited at 488 nm; laser power 20%; exposure time 300 ms). Imaging started at 12 hpf with a 30-minute interval over 16.5 hours. Scale bar = 200 μm.

Movie S3. Wide-field time-lapse confocal imaging of neural network formation in the brain and yolk sac of a zebrafish (elavl3:EGFP) embryo. Images were acquired using a 30x silicon oil-immersion objective. Pan-neuronal structures are labeled with EGFP (488 nm excitation; 20% laser power; 200 ms exposure). Time-lapse imaging started at 24 hpf with a 20-minute interval for over 38 hours. Scale bar = 50 μm.

Movie S4. Wide-field time-lapse confocal imaging of ventral primary neuron growth toward the spinal cord in a zebrafish (elavl3:EGFP) embryo. Images were acquired using a 10x objective. Pan-neuronal structures are labeled with EGFP (488 nm excitation; 20% laser power; 300 ms exposure). Imaging started at 24 hpf with a 20-minute interval for over 22 hours. Scale bar = 50 μm.

Movie S5. Time-lapse confocal imaging of blood cell circulation in a zebrafish embryo. Images were acquired using a 30x silicon oil-immersion objective. Imaging started at 24 hpf with a 1-second interval. The left panel shows blood flow in the brain, the middle panel shows circulation on the yolk sac surface, and the right panel shows spinal cord blood flow. Scale bar = 50 μm.

Movie S6. High-magnification time-lapse confocal imaging of neural network formation in a zebrafish (elavl3:EGFP) embryo. Images were acquired using a 60x oil-immersion objective. Pan-neuronal structures are labeled with EGFP (488 nm excitation; 20% laser power; 200 ms exposure). Imaging started at 24 hpf with a 20-minute interval over 47 hours. Scale bar = 20 μm.

Movie S7. Wide-field time-lapse confocal imaging of neural network formation in the spinal cord of a zebrafish (elavl3:EGFP) embryo. Images were acquired using a 30x silicon oil-

immersion objective. Pan-neuronal structures are labeled with EGFP (488 nm excitation; 20% laser power; 200 ms exposure). Imaging started at 24 hpf with a 10-minute interval for over 8.5 hours. Scale bar = 50 μm.

Movie S8. Wide-field time-lapse confocal imaging of neural network refinement in a zebrafish (elavl3:CaMP6f) embryo. Images were acquired using a 30x silicon oil-immersion objective. Calcium signals in pan-neuronal structures are indicated by CaMP6f (488 nm excitation; 20% laser power; 200 ms exposure). The left video started at 33.5 hpf with a 25-minute interval; the right video started at 50 hpf with a 10-minute interval. Scale bar = 50 μm.

Movie S9. Wide-field time-lapse confocal imaging of somatic calcium transients in the brain of a zebrafish (elavl3:CaMP6f) embryo. Images were acquired using a 30x silicon oil-immersion objective. Calcium signals in pan-neuronal structures are indicated by CaMP6f (488 nm excitation; 20% laser power; 200 ms exposure). The left video started at 24 hpf; the right video started at 52 hpf. Both were acquired with a 0.491-second interval. Scale bar = 50 μm.

Movie S10. Wide-field time-lapse confocal imaging of neural transport in zebrafish embryos. Images were acquired using a 30x silicon oil-immersion objective (488 nm excitation; 20% laser power; 200 ms exposure). Left: Zebrafish (elavl3:CaMP6f) showing calcium signals in pan-neuronal structures. Imaging started at 50 hpf with a ~4-second interval. Right: Zebrafish (elavl3:EGFP) with EGFP-labeled pan-neuronal structures. Imaging started at 48 hpf with a ~10-minute interval. Scale bar = 50 μm.

Captions for Supplementary Figures.

Figure S1.The fluorescently labeled transgenetic zebrafish line. a, Representative confocal image of a zebrafish (fli-1:mCherry) embryo. Red fluorescence labels vascular endothelium. The left panel shows the entire embryo; scale bar = 200 μm. The right panel shows a magnified view; scale bar = 50 μm. **b,** Representative confocal image of a zebrafish (elavl3:EGFP) embryo. Green fluorescence labels pan-neuronal structures. The left panel shows the entire embryo; scale bar = 200 μm. The right panel shows a magnified view; scale bar = 50 μm. **c,** Representative confocal image of a zebrafish (cldnb:lynEGFP) embryo. Green fluorescence labels the lateral line system. The left panel shows the entire embryo; scale bar = 200 μm. The right panel shows a magnified view; scale bar = 50 μm. **d,** Representative confocal image of a zebrafish (cmlc2:EGFP) embryo. Green fluorescence labels cardiac muscle. The left panel shows the entire embryo; scale bar = 200 μm. The right panel shows a magnified view; scale bar = 50 μm. **e,** Representative confocal image of a zebrafish (smyhc1:EGFP) embryo. Green fluorescence labels skeletal muscle. The left panel shows the entire embryo; scale bar = 200 μm. The right panel shows a magnified view; scale bar = 50 μm. **f,** Representative confocal image of a zebrafish (elavl3:CaMP6f) embryo. Green fluorescence reflects neuronal calcium activity. The left panel shows the entire embryo; scale bar

1109 = 200 μm. The right panel shows a magnified view; scale bar = 50 μm.
1110
1111 **Figure S2. Imaging reconstruction and data analysis. a,** Representative image of a three-
1112 dimensional reconstruction of the embryonic neural network in zebrafish, generated using
1113 CellSens Dimension Desktop software (version 4.2.1).
1114
1115 **Figure S3. Transcriptomic analysis of zebrafish embryos at different developmental time**
1116 **points. a,** Genome-wide Mfuzz time-series gene clustering analysis of zebrafish embryos across
1117 various developmental stages. **b,** Heatmap and corresponding expression trend profiles of genome-
1118 wide transcriptome dynamics during zebrafish embryonic development.

Fig1

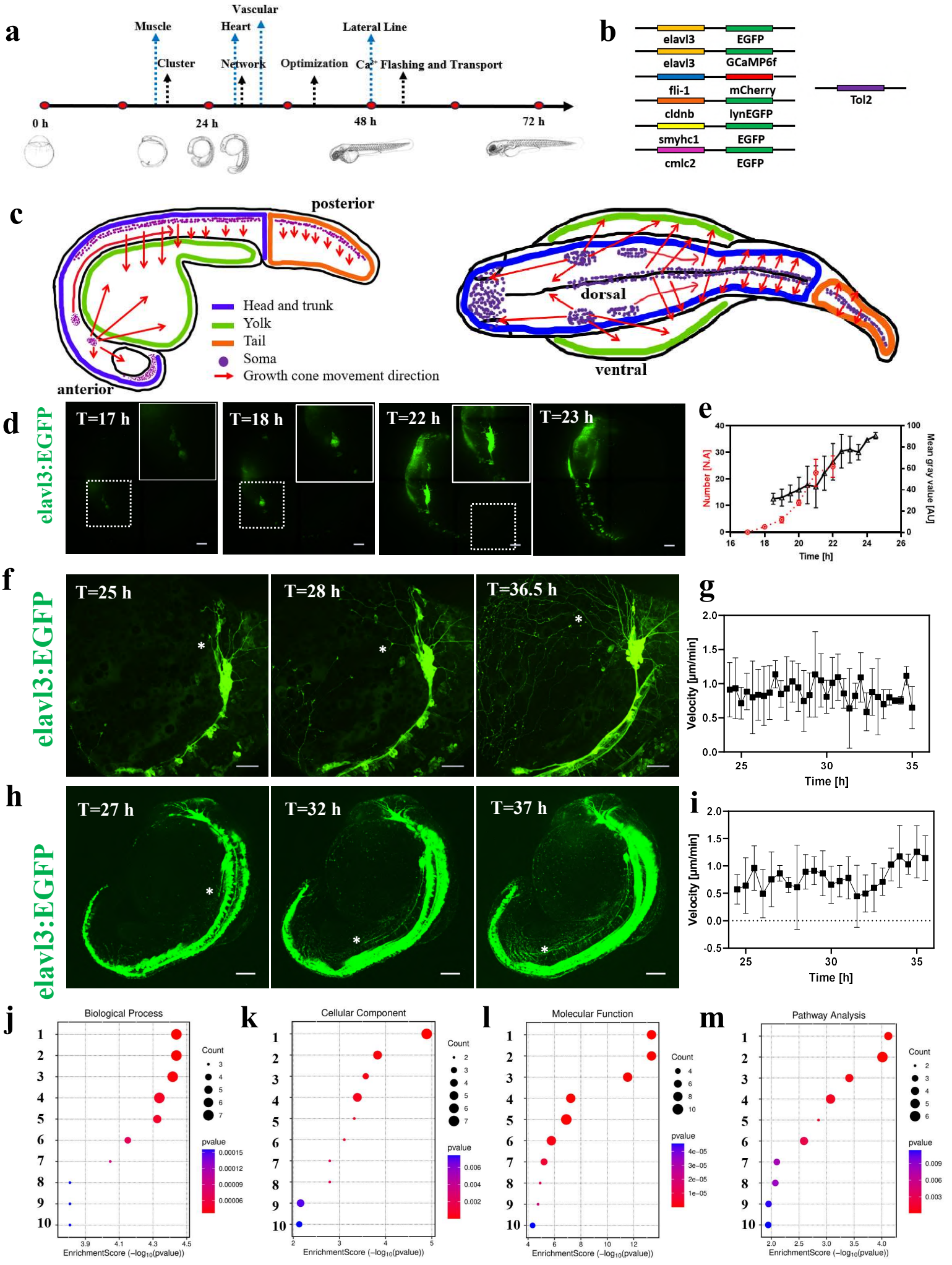
a
Muscle
Vascular
Heart
Lateral Line
Cluster
Network
Optimization
Ca2+ Flashing and Transport
0 h
24 h
48 h
72 h
b
elavl3
EGFP
elavl3
GCaMP6f
fli-1
mCherry
cldnb
lynEGFP
smyhc1
EGFP
cmlc2
EGFP
Tol2
c
posterior
anterior
dorsal
ventral
Head and trunk
Yolk
Tail
Soma
Growth cone movement direction
d
elavl3:EGFP
T=17 h
T=18 h
T=22 h
T=23 h
e
Number [N.A]
Mean gray value [AU]
Time [h]
f
elavl3:EGFP
T=25 h
T=28 h
T=36.5 h
g
Velocity [μm/min]
Time [h]
h
elavl3:EGFP
T=27 h
T=32 h
T=37 h
i
Velocity [μm/min]
Time [h]
j
Biological Process
Count
pvalue
EnrichmentScore (−log10(pvalue))
k
Cellular Component
Count
pvalue
EnrichmentScore (−log10(pvalue))
l
Molecular Function
Count
pvalue
EnrichmentScore (−log10(pvalue))
m
Pathway Analysis
Count
pvalue
EnrichmentScore (−log10(pvalue))

Fig2

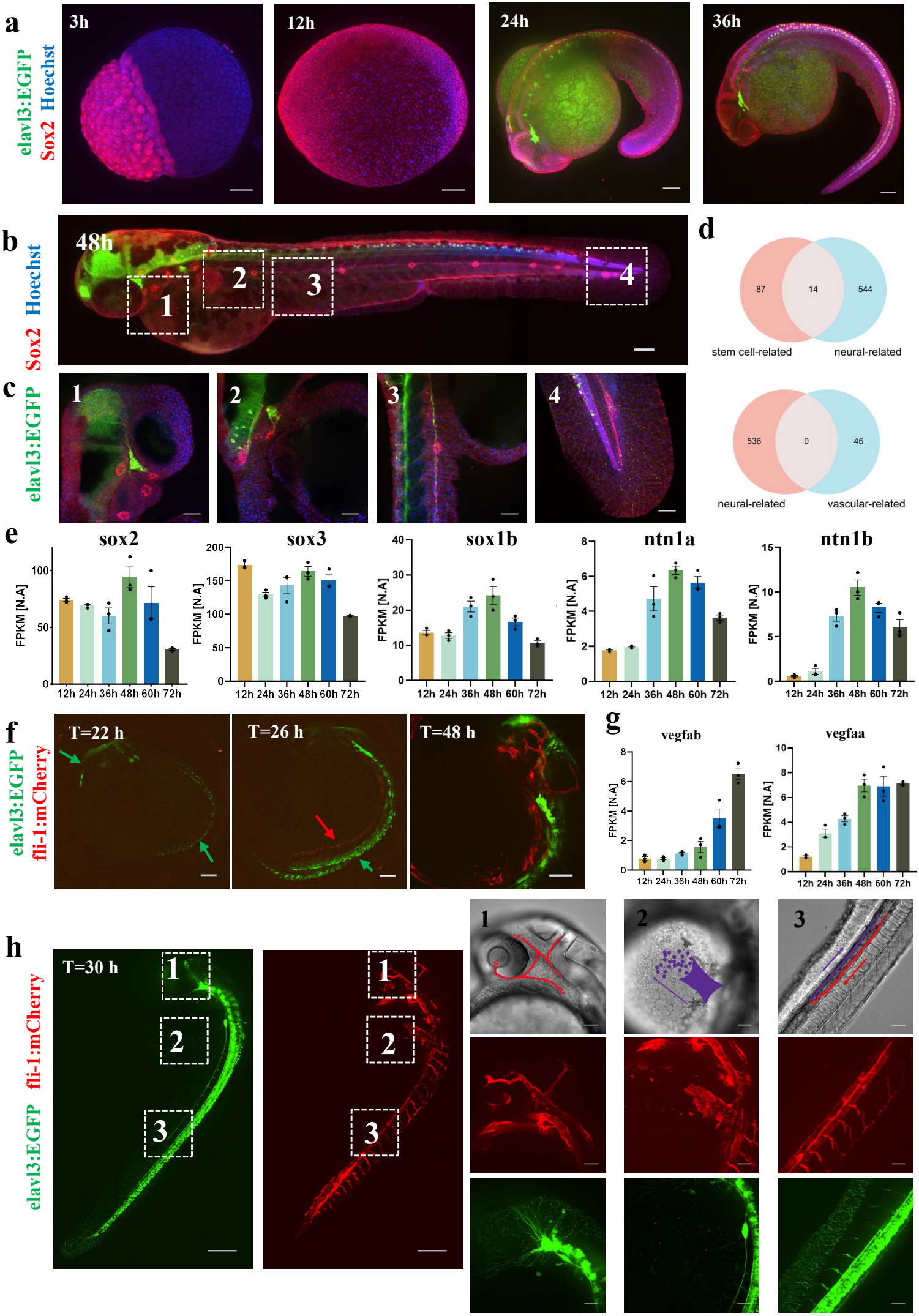
a
elavl3:EGFP
Sox2
Hoechst
3h
12h
24h
36h
b
Hoechst
Sox2
48h
1
2
3
4
c
elavl3:EGFP
d
87
14
544
stem cell-related
neural-related
536
0
46
neural-related
vascular-related
e
sox2
sox3
sox1b
ntn1a
ntn1b
FPKM [N.A]
12h 24h 36h 48h 60h 72h
f
elavl3:EGFP
fli-1:mCherry
T=22 h
T=26 h
T=48 h
g
vegfab
vegfaa
h
elavl3:EGFP
fli-1:mCherry
T=30 h

Fig3

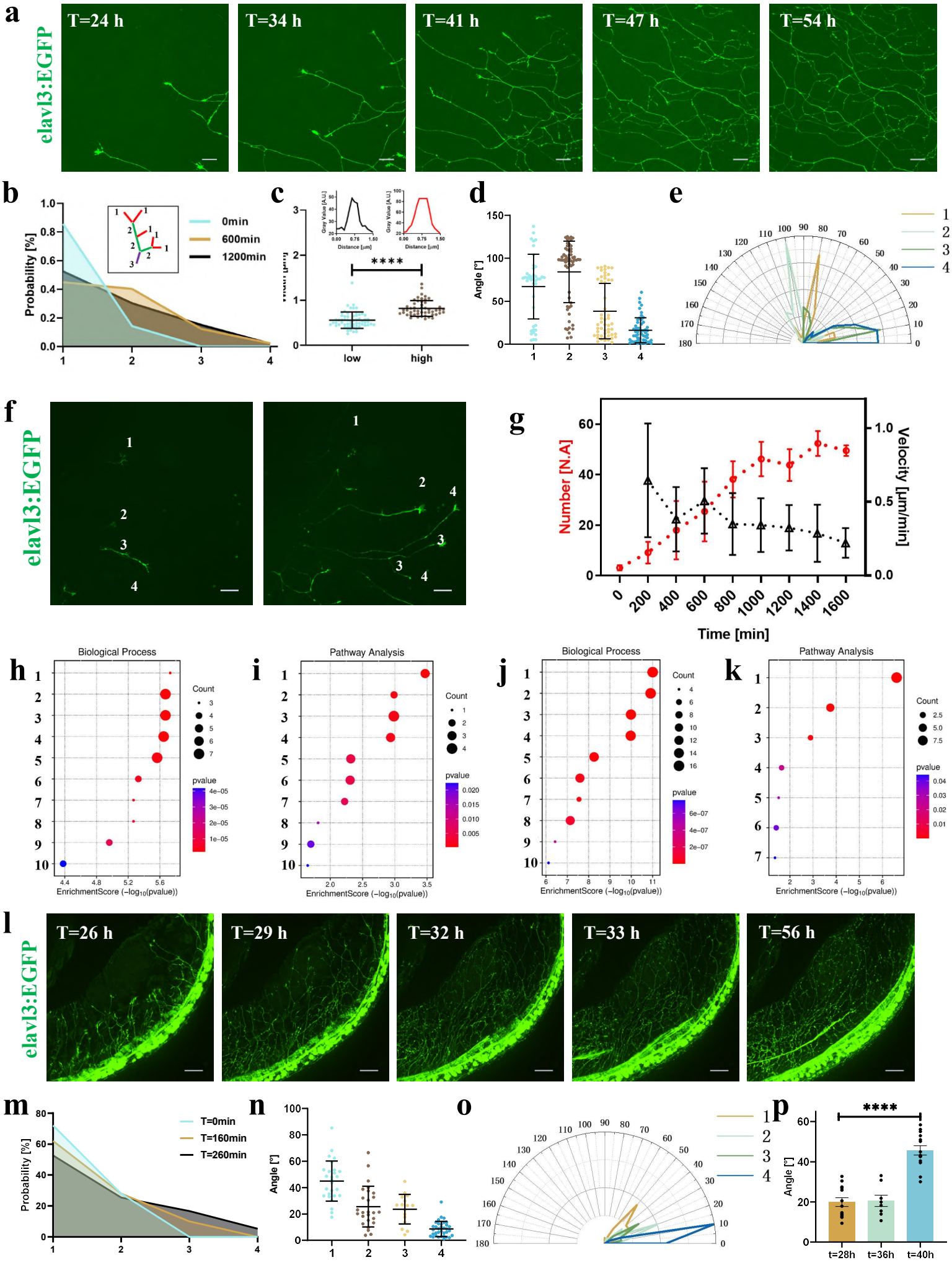
a
elavl3:EGFP
T=24 h
T=34 h
T=41 h
T=47 h
T=54 h
b
Probability [%]
0min
600min
1200min
c
Gray Value [A.U.]
Distance [μm]
****
low
high
d
Angle [°]
e
f
elavl3:EGFP
g
Number [N.A]
Velocity [μm/min]
Time [min]
h
Biological Process
EnrichmentScore (−log10(pvalue))
Count
pvalue
i
Pathway Analysis
j
Biological Process
k
Pathway Analysis
l
elavl3:EGFP
T=26 h
T=29 h
T=32 h
T=33 h
T=56 h
m
Probability [%]
T=0min
T=160min
T=260min
n
Angle [°]
o
p
Angle [°]
****
t=28h
t=36h
t=40h

Fig4

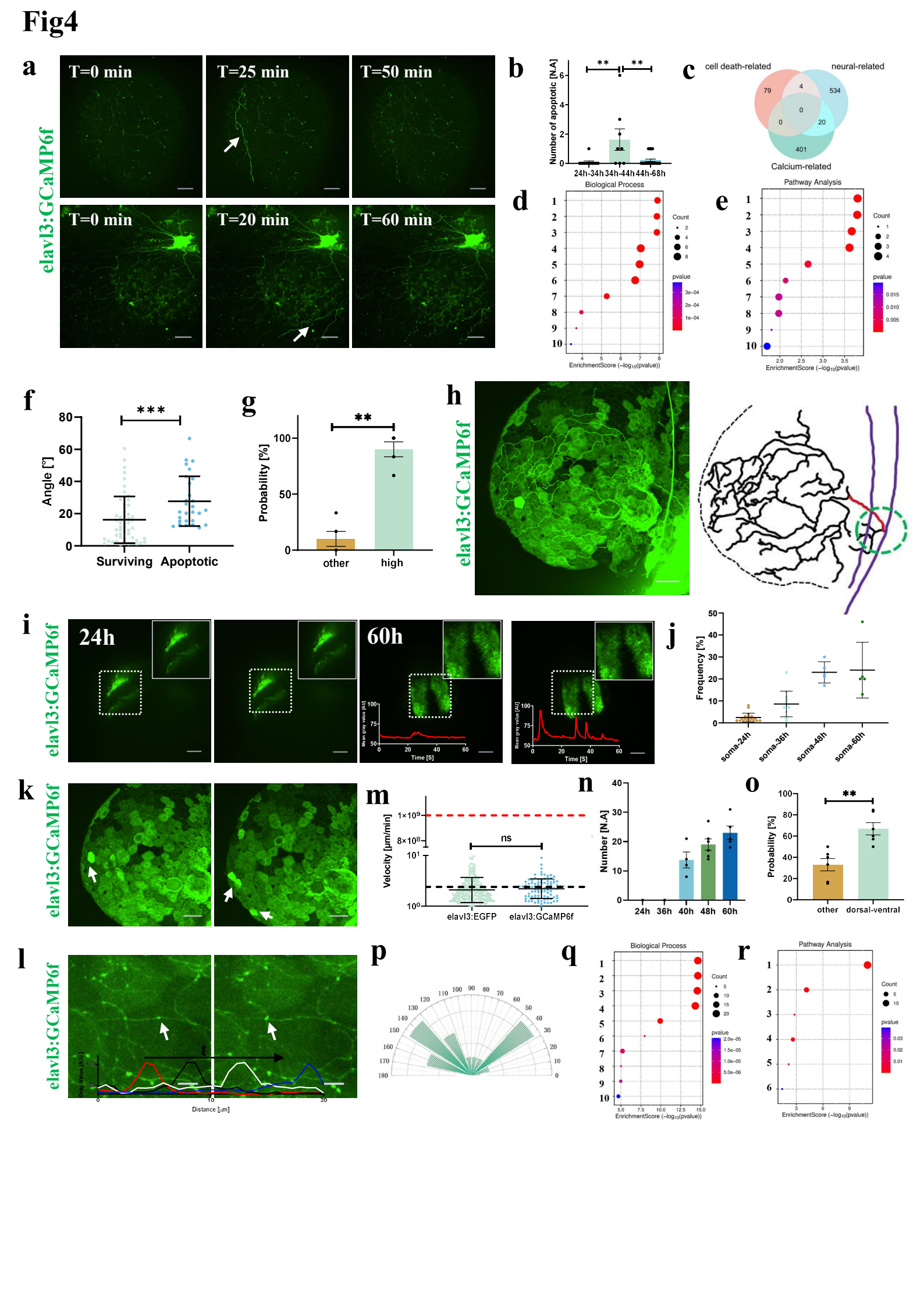
a
elavl3:GCaMP6f
T=0 min
T=25 min
T=50 min
T=0 min
T=20 min
T=60 min
b
Number of apoptotic [N.A]
24h-34h
34h-44h
44h-68h
c
cell death-related
neural-related
Calcium-related
79
4
534
0
0
20
401
d
Biological Process
Count
pvalue
EnrichmentScore (−log10(pvalue))
e
Pathway Analysis
Count
pvalue
EnrichmentScore (−log10(pvalue))
f
Angle [°]
Surviving
Apoptotic
g
Probability [%]
other
high
h
elavl3:GCaMP6f
i
elavl3:GCaMP6f
24h
60h
Time [S]
j
Frequency [%]
soma-24h
soma-36h
soma-48h
soma-60h
k
elavl3:GCaMP6f
m
Velocity [µm/min]
ns
elavl3:EGFP
elavl3:GCaMP6f
n
Number [N.A]
24h
36h
40h
48h
60h
o
Probability [%]
other
dorsal-ventral
l
elavl3:GCaMP6f
Distance [µm]
p
q
Biological Process
Count
pvalue
EnrichmentScore (−log10(pvalue))
r
Pathway Analysis
Count
pvalue
EnrichmentScore (−log10(pvalue))

Extended Data Figure 1

1. Imaging Sample Preparation

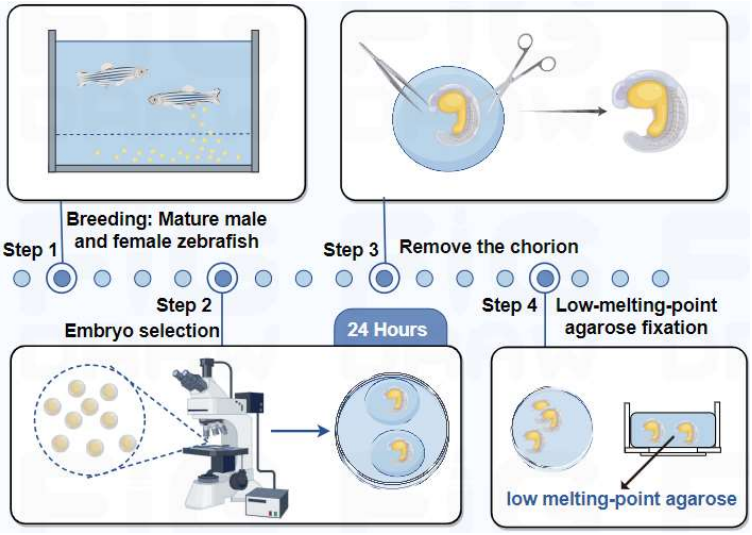

2. Live Cell Imaging

3. Analysis of Neural Network Formation

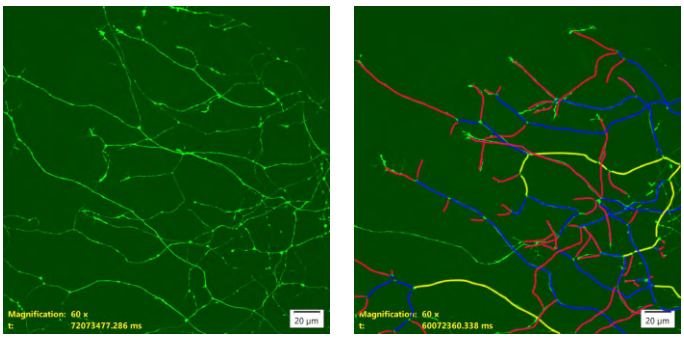

4. Molecular Biological Analysis

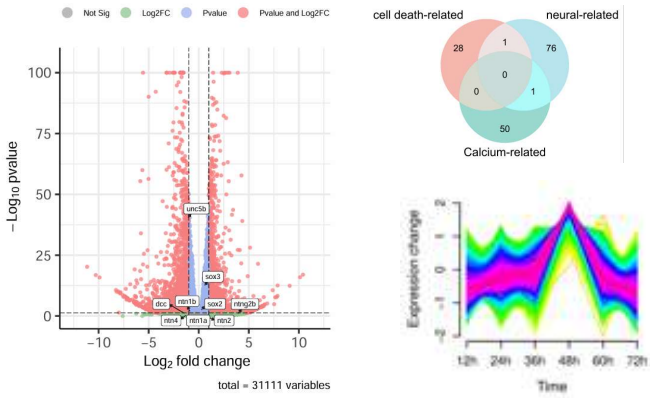

Extended Data Figure 2

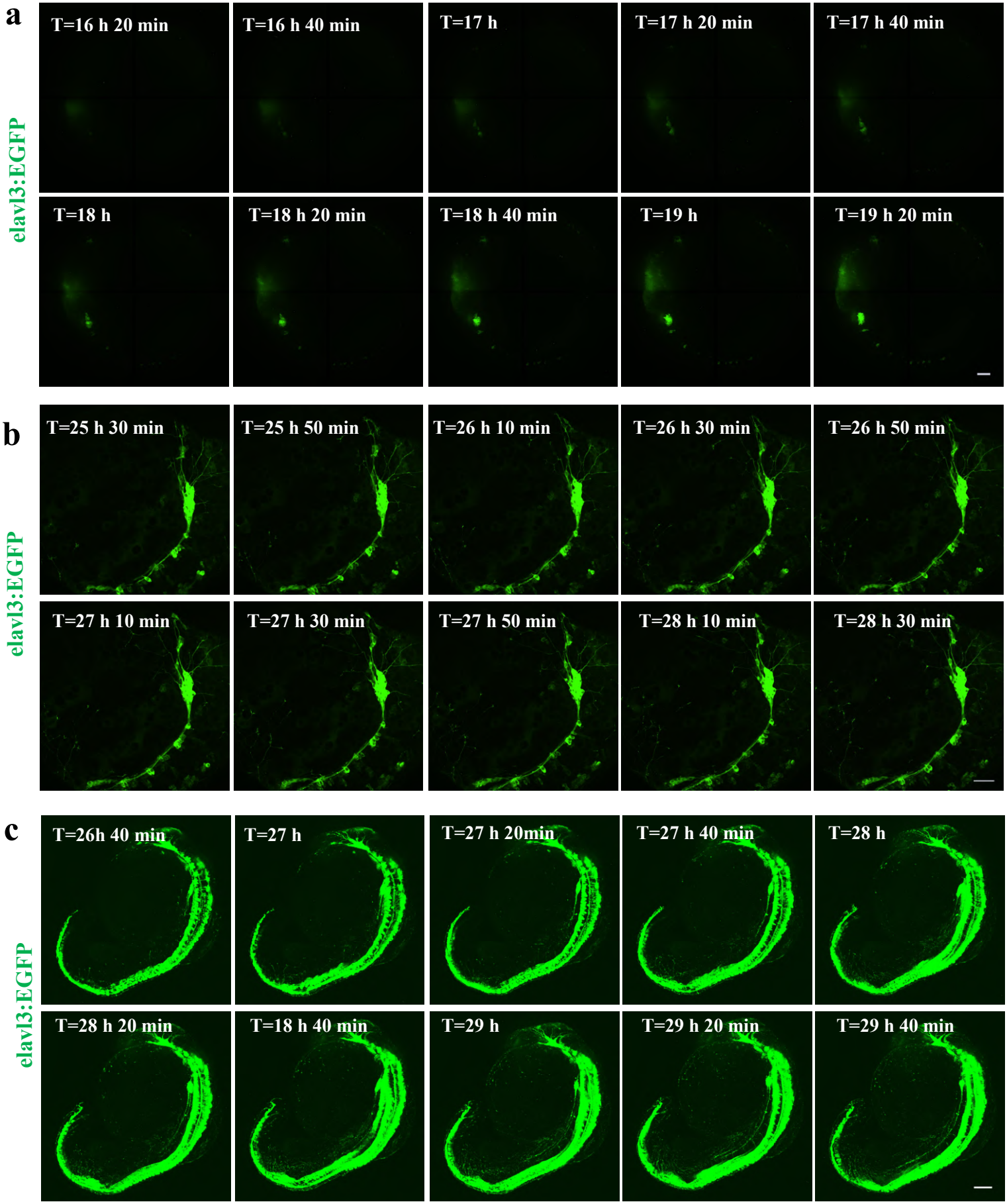

Extended Data Figure 3

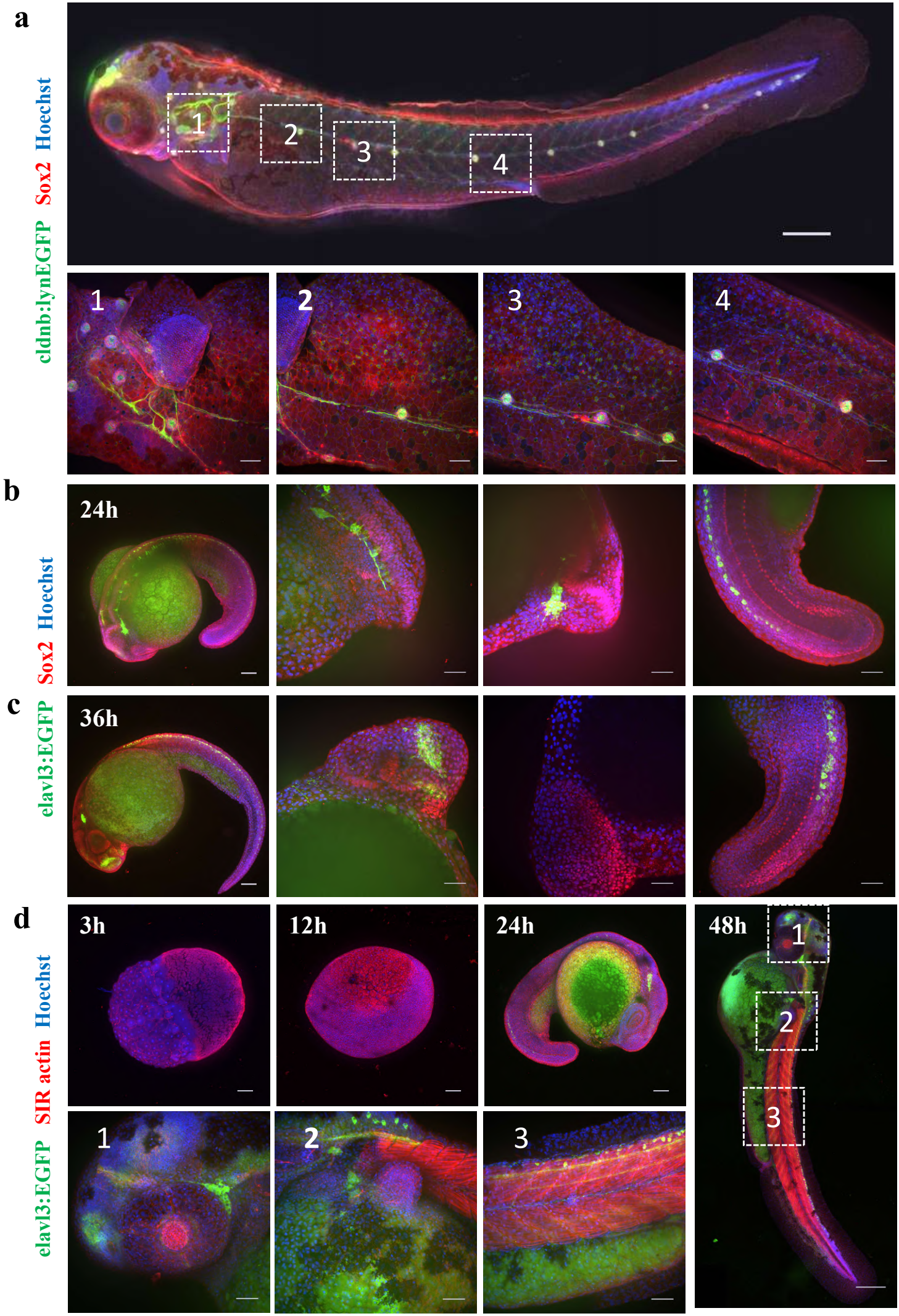

Extended Data Figure 4

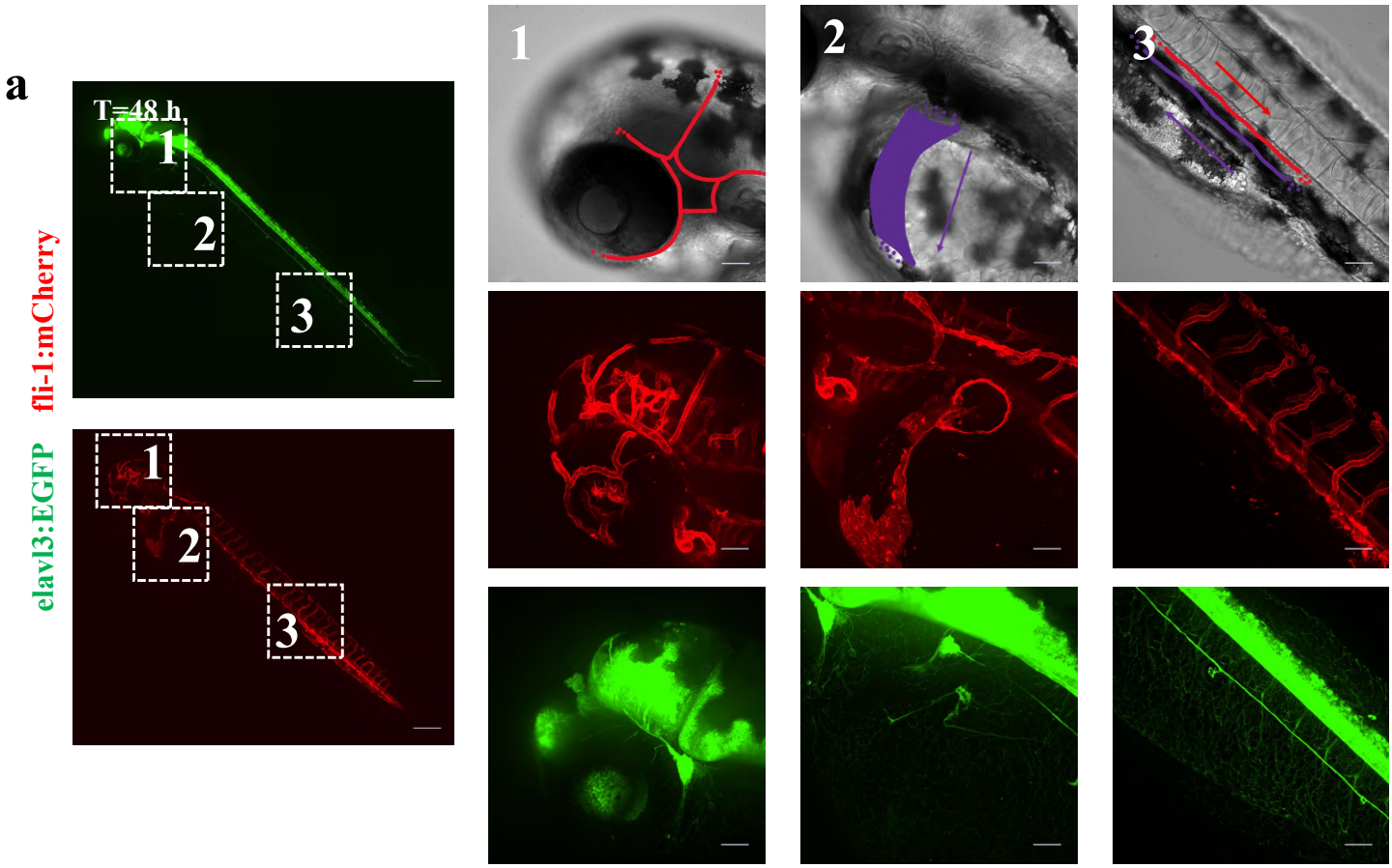

Extended Data Figure 5

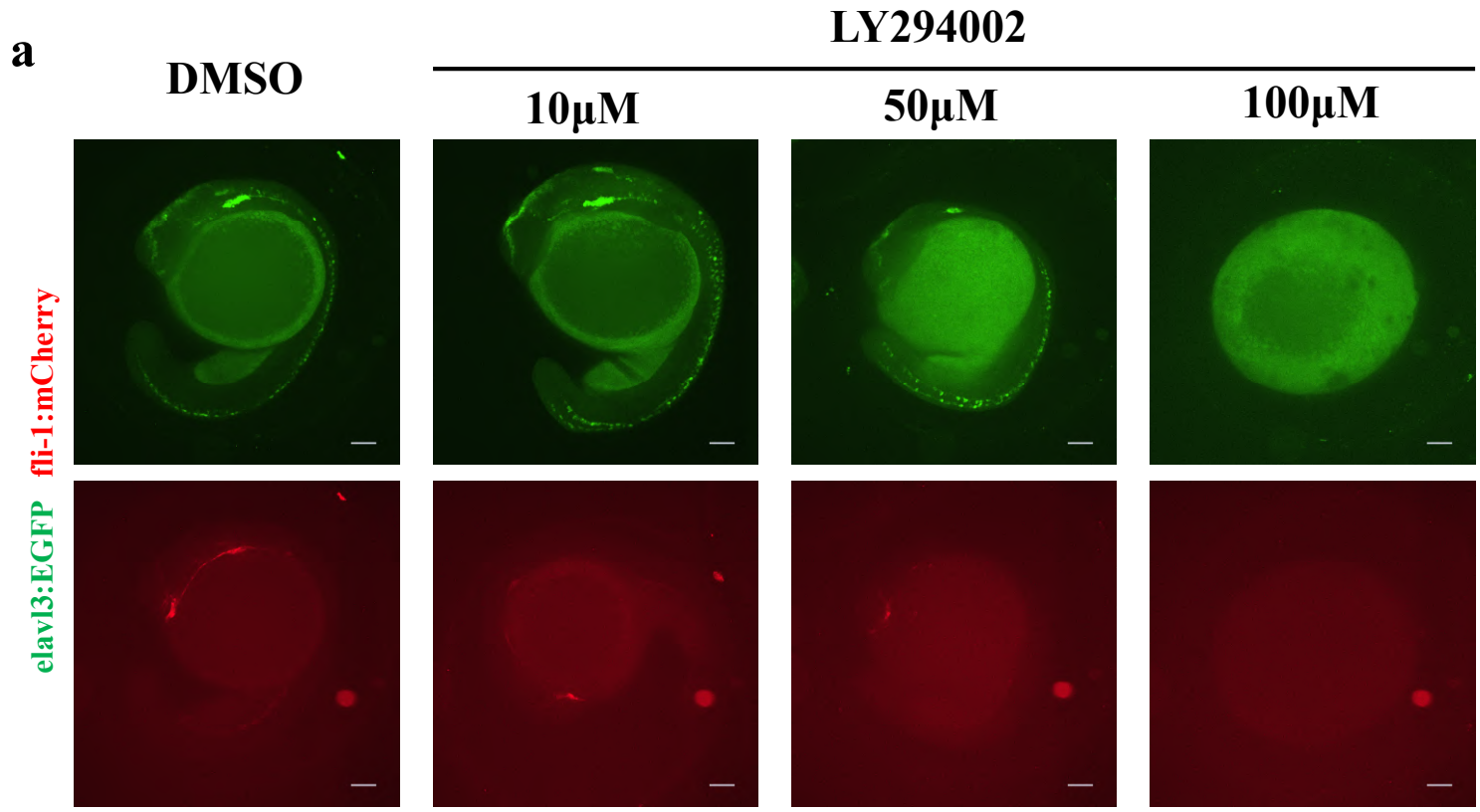

Extended Data Figure 6

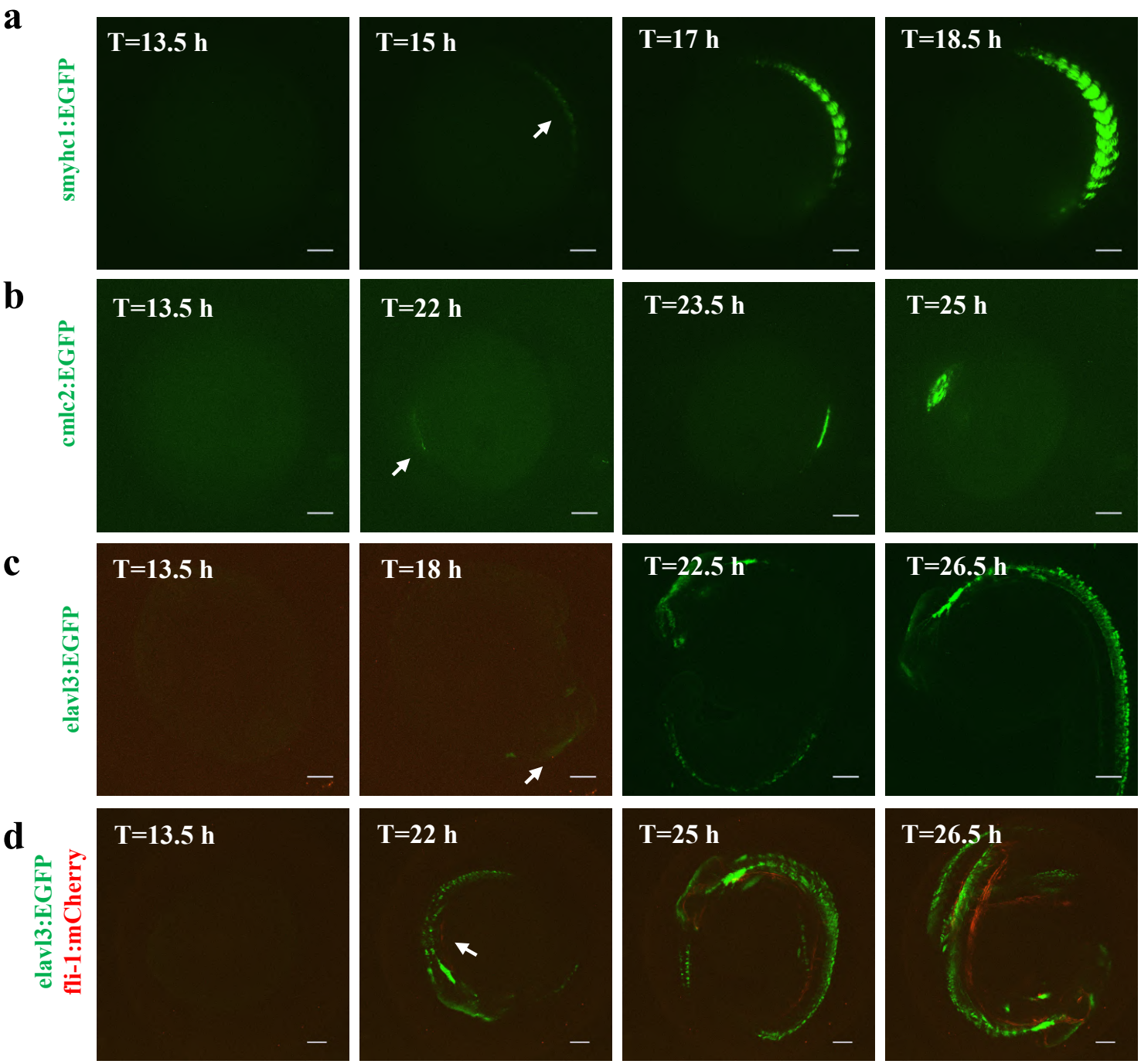

Extended Data Figure 7

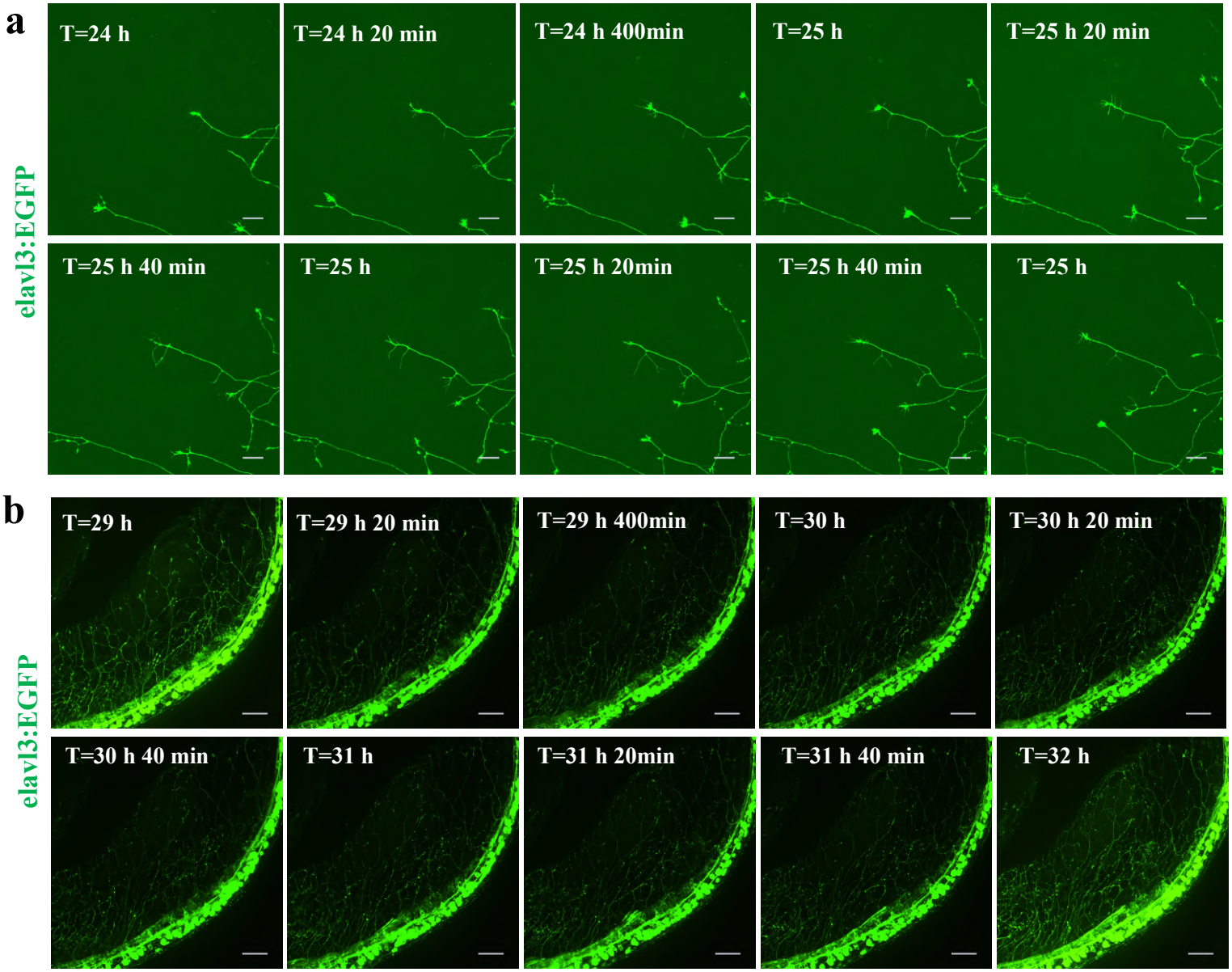

Extended Data Figure 8

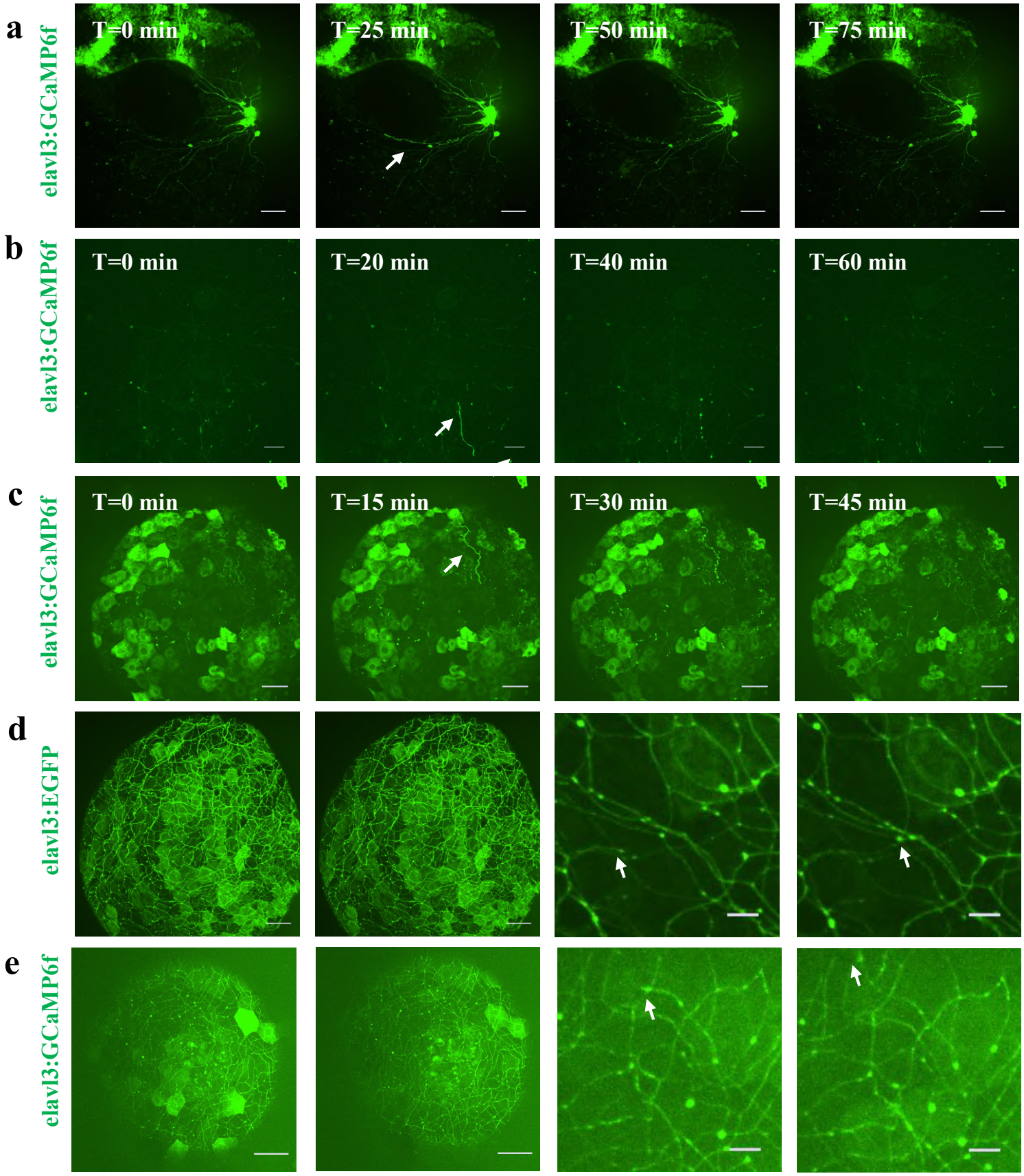

Extended Data Figure 9

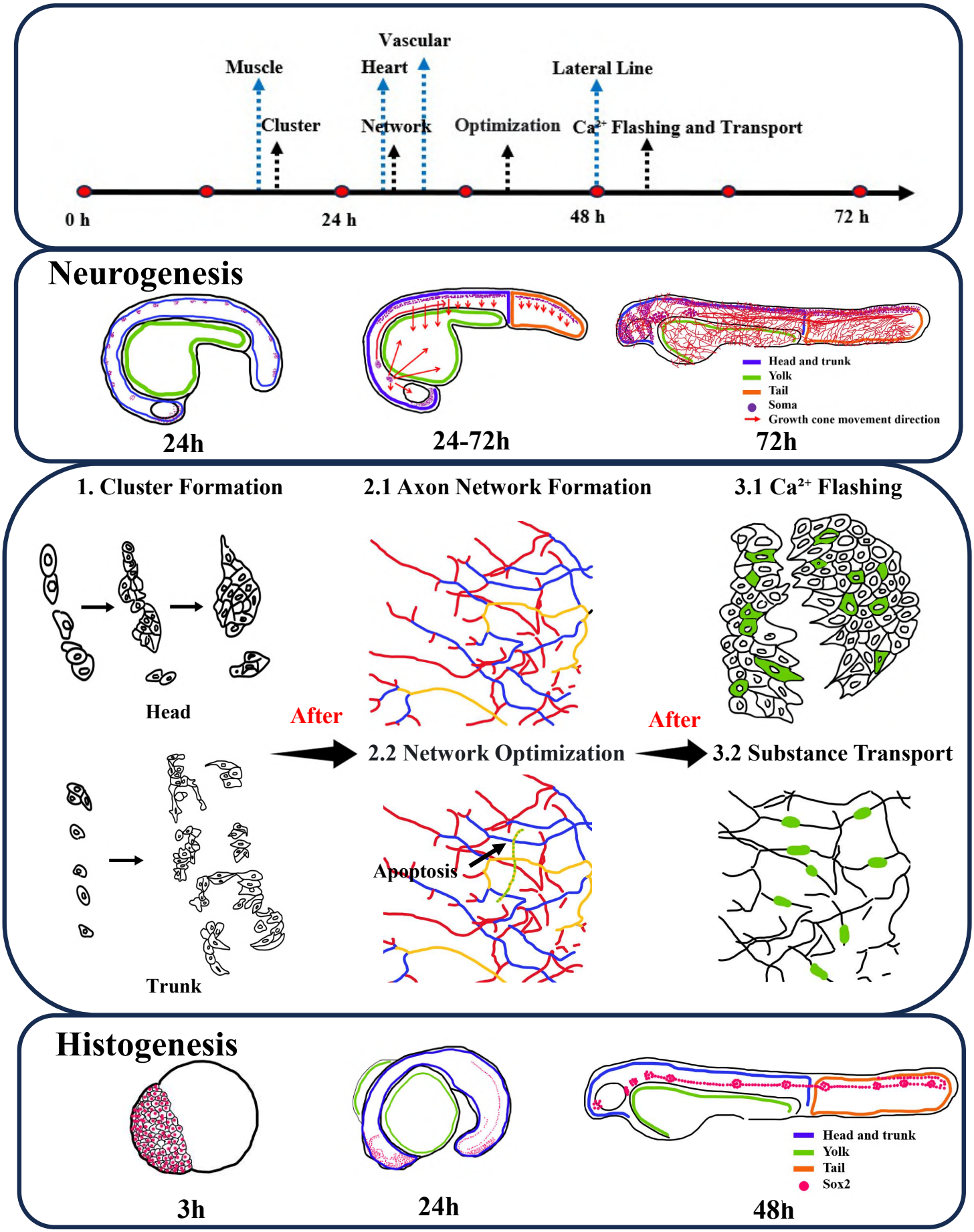

Fig. S1

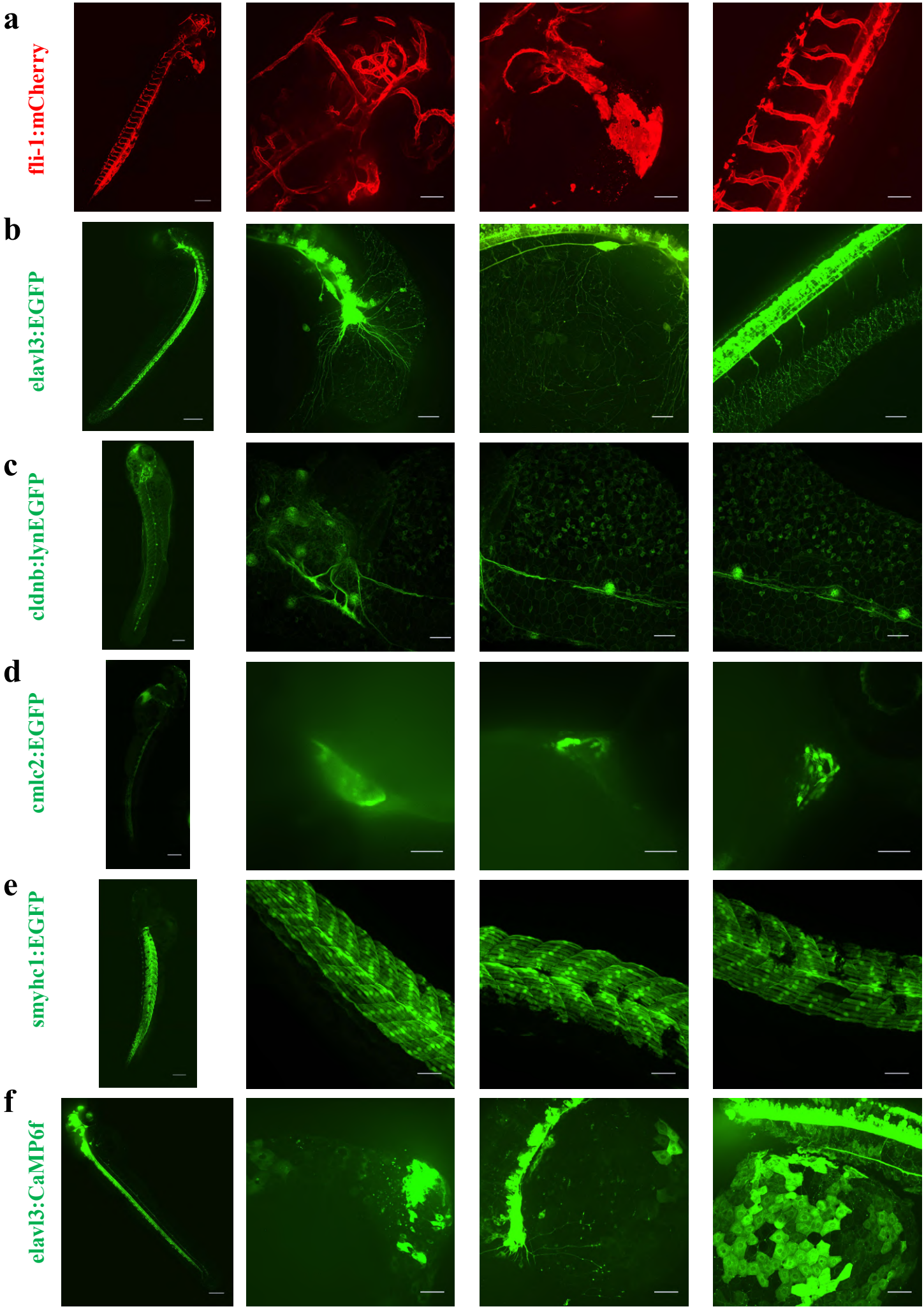
a
fli-1:mCherry
b
elavl3:EGFP
c
cldnb:lynEGFP
d
cmlc2:EGFP
e
smyhc1:EGFP
f
elavl3:CaMP6f

Fig. S2

a

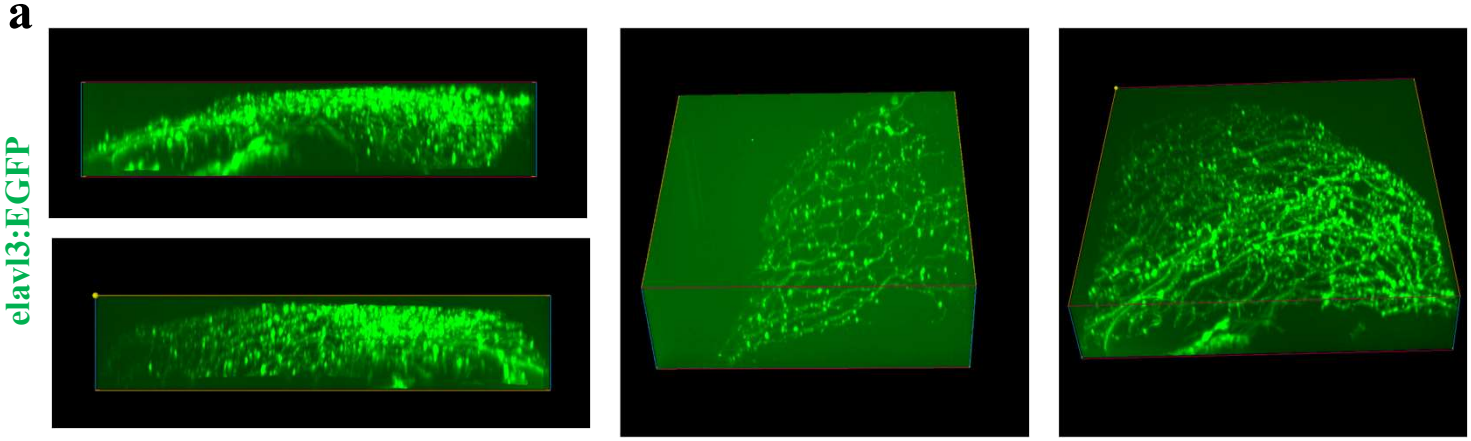

Fig. S3

a

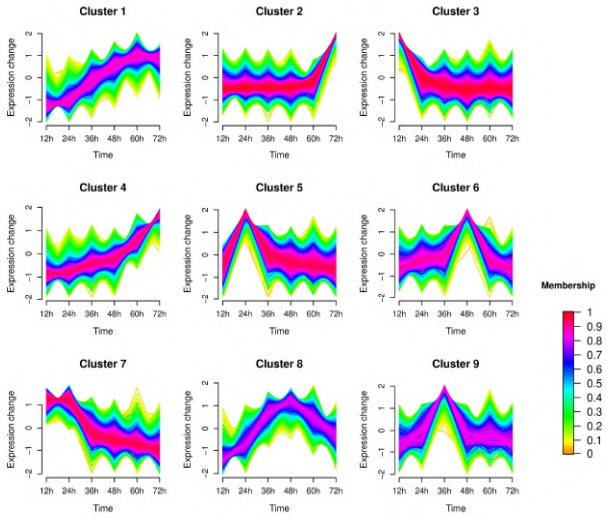
Cluster 1
Cluster 2
Cluster 3
Cluster 4
Cluster 5
Cluster 6
Cluster 7
Cluster 8
Cluster 9
Expression change
Time
12h 24h 36h 48h 60h 72h
Membership
1
0.9
0.8
0.7
0.6
0.5
0.4
0.3
0.2
0.1
0

b

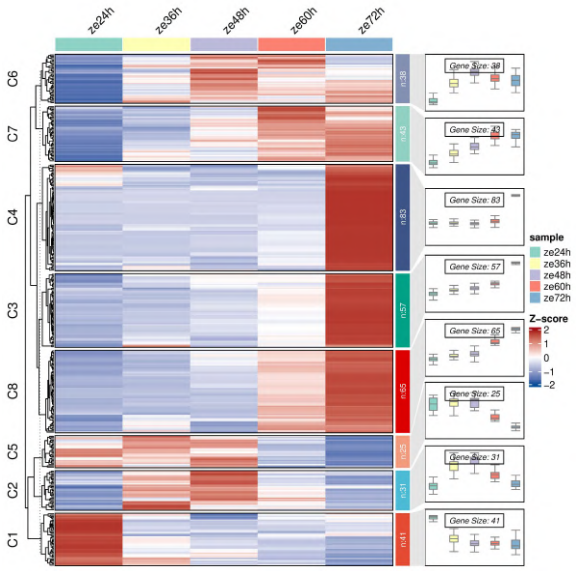
ze24h
ze36h
ze48h
ze60h
ze72h
C1
C2
C5
C8
C3
C4
C7
C6
n:41
n:31
n:25
n:65
n:57
n:83
n:43
n:38
Gene Size: 41
Gene Size: 31
Gene Size: 25
Gene Size: 65
Gene Size: 57
Gene Size: 83
Gene Size: 43
Gene Size: 38
sample
ze24h
ze36h
ze48h
ze60h
ze72h
Z-score
2
1
0
−1
−2